Article

R9AP is a common receptor for EBV infection in epithelial cells and B cells

https://doi.org/10.1038/s41586-025-09166-w

Received: 22 November 2020

Accepted: 15 May 2025

Published online: 18 June 2025

Open access

Check for updates

Yan Li[1,2,10], Hua Zhang[3,10], Cong Sun[1,10], Xiao-Dong Dong[1,10], Chu Xie[1], Yuan-Tao Liu[1], Ruo-Bin Lin[1], Xiang-Wei Kong[1], Zhu-Long Hu[1], Xiao-Yan Ma[1], Dan-Ling Dai[1], Qian-Ying Zhu[1], Yu-Chun Li[3], Ying Li[3], Shang-Xin Liu[1], Li Yuan[1], Peng-Hui Zhou[1], Song Gao[1], Ya-Ping Tang[4], Jin-Ying Yang[4], Ping Han[5], Andrew T. McGuire[6], Bo Zhao[7], Jin-Xin Bei[1], Erle Robertson[8], Yi-Xin Zeng[1], Qian Zhong[1] ✉ & Mu-Sheng Zeng[1,9] ✉

Epstein–Barr virus (EBV) persistently infects more than 90% of the human population, causing infectious mononucleosis[1], susceptibility to autoimmune diseases[2] and multiple malignancies of epithelial or B cell-origin[3]. EBV infects epithelial cells and B cells through interaction between viral glycoproteins and different host receptors[4], but it has remained unknown whether a common receptor mediates infection of its two major host cell targets. Here, we establish R9AP as a crucial EBV receptor for entry into epithelial and B cells. R9AP silencing or knockout, R9AP-derived peptide and R9AP monoclonal antibody each significantly inhibit, whereas R9AP overexpression promotes, EBV uptake into both cell types. R9AP binds directly to the EBV glycoprotein gH/gL complex to initiate gH/gL–gB-mediated membrane fusion. Notably, the interaction of R9AP with gH/gL is inhibited by the highly competitive gH/gL-neutralizing antibody AMMO1, which blocks EBV epithelial and B cell entry. Moreover, R9AP mediates viral and cellular membrane fusion in cooperation with EBV gp42–human leukocyte antigen class II or gH/gL–EPHA2 complexes in B cells or epithelial cells, respectively. We propose R9AP as the crucial common receptor of B cells and epithelial cells and a potential prophylactic and vaccine target for EBV.

The oncogenic gammaherpesvirus EBV is highly tropic for B cells and epithelial cells[5]. EBV causes 200,000 cancers per year, approximately evenly divided between B cell and epithelial cell malignancies[6]. EBV is highly associated with Burkitt, Hodgkin and post-transplant B cell lymphomas, nasopharyngeal carcinoma and gastric carcinoma[6]. It has been suggested that EBV uses multiple viral glycoproteins and distinct host receptors to infect human epithelial cells versus B cells[4]. EBV attachment to B cells depends on the interaction between gp350 and the complement receptor type 2 (CR2 (also known as CD21)) or CD35[7,8]. Gp42, in complex with gH/gL, interacts with human leukocyte antigen (HLA) class II to trigger the EBV fusogen gB to drive B cell entry[9–11]. By contrast, EBV epithelial cell infection is more complex. As core fusion machinery members[12], gH/gL and gB are also required for epithelial cell infection. However, although critical for uptake in B cells, gp42 inhibits EBV infection of epithelial cells[13,14]. Furthermore, epithelial cells do not typically express CR2, CD35 or HLA class II[4,15,16]. Instead, EPHA2, NRP1, integrins and non-muscle myosin heavy chain IIA (also known as myosin-9) have been suggested to drive EBV epithelial cell infection via a multistep process[16–20]. Nonetheless, the gH/gL-neutralizing antibody AMMO1 blocks EBV infection in both epithelial cells and B cells[21,22], suggesting a potential shared mechanism of EBV uptake, potentially at the level of an unidentified common cellular receptor or other entry mediator. Here, we describe R9AP (encoded by *RGS9BP*) as a key receptor for EBV infection of epithelial and B cells, whose interaction with gH/gL is disrupted by AMMO1.

Screen identifies R9AP in EBV infection

Since EBV infection efficiency of immortalized nasopharyngeal epithelial cells (NPECs) is significantly higher when cultured as sphere-like cells (SLCs) than as monolayer cells (MLCs)[16], we hypothesized that unidentified EBV receptor(s) might be expressed at higher levels in SLCs than MLCs. We therefore performed genome-wide microarray analysis to identify genes that are differentially expressed between SLCs and MLCs (Extended Data Fig. 1a and Supplementary Table 1). Then, we screened EBV transcripts that were more highly expressed in SLCs by short interfering RNA (siRNA) silencing to investigate their roles in EBV entry. This identified four candidates, CNGA1, GPR1, SLC26A9 and R9AP, whose

[1]State Key Laboratory of Oncology in South China, Guangdong Key Laboratory of Nasopharyngeal Carcinoma Diagnosis and Therapy, Sun Yat-sen University Cancer Center, Guangzhou, China. [2]Department of Pathology, Sun Yat-sen University Cancer Center, Guangzhou, China. [3]MOE Key Laboratory of Tropical Disease Control, Centre for Infection and Immunity Studies (CIIS), School of Medicine, Sun Yat-sen University, Shenzhen, China. [4]Guangdong Province Key Laboratory of Structural Birth Defect, Guangzhou Institute of Pediatrics, Guangzhou Women and Children's Medical Center, Guangzhou Medical University, Guangzhou, China. [5]Department of Otolaryngology, Head and Neck Surgery, Sun Yat-sen Memorial Hospital, Sun Yat-sen University, Guangzhou, China. [6]Vaccine and Infectious Disease Division, Fred Hutchinson Cancer Research Center, Seattle, WA, USA. [7]Department of Medicine, Brigham and Women's Hospital, Harvard Medical School, Boston, MA, USA. [8]Department of Otorhinolaryngology, Head and Neck Surgery and Microbiology, Perelman School of Medicine, University of Pennsylvania, Philadelphia, PA, USA. [9]Guangdong-Hong Kong Joint Laboratory for RNA Medicine, Sun Yat-Sen University, Guangzhou, China. [10]These authors contributed equally: Yan Li, Hua Zhang, Cong Sun, Xiao-Dong Dong. ✉e-mail: zhongqian@sysucc.org.cn; zengmsh@sysucc.org.cn

knockdown reduced NPEC infection by more than 50% when grown as SLCs (Extended Data Fig. 1b,c). Immunoblot analysis revealed that CNGA1 and R9AP, but not GPR1 or SLC26A9, were expressed across all cell lines that were susceptible to EBV infection (Extended Data Fig. 1d). However, overexpression of R9AP, but not CNGA1, increased EBV infection by nearly threefold compared with control empty vector (Extended Data Fig. 1e,f). Results of the screen are summarized in Extended Data Fig. 1g. Quantitative PCR with reverse transcription (RT–qPCR) and flow cytometry analysis further verified R9AP expression in multiple EBV-infected epithelial and B cell lines (Extended Data Fig. 2a,b). Together, these data suggest a potential role of R9AP in EBV infection.

R9AP has a key role in EBV infection

To explore a potential role for R9AP in epithelial cell infection, we challenged control or R9AP-depleted HNE1 nasopharyngeal cells with recombinant EBV that encodes a GFP reporter. siRNA-mediated knockdown of R9AP significantly diminished EBV infection, as judged by reduced GFP expression at 24 h post-EBV co-incubation (Fig. 1a,b and Extended Data Fig. 2c). Consistent with this analysis, CRISPR–Cas9-mediated R9AP depletion using independent single guide RNAs (sgR9AP 1 or sgR9AP 2) significantly reduced EBV infection rates compared with control cells (Fig. 1c and Extended Data Fig. 2d). Notably, EBV infection efficiency of R9AP-knockout cells (sgR9AP 1) was significantly restored by rescue R9AP expression (Fig. 1d and Extended Data Fig. 2e), indicating on-target CRISPR effects on EBV uptake. Of note, EBV infection was almost completely abolished in single-cell R9AP-knockout HNE1 clones (Fig. 1e,f), in which EBV gene expression was undetectable at 72 h after co-incubation (Extended Data Fig. 2f–h). Consistently, EBV infection efficiency of R9AP-knockout HNE1 clone (clone 1) was significantly restored by rescue R9AP expression (Extended Data Fig. 2i,j). Similar R9AP-knockout and cDNA rescue assay phenotypes were observed in AGS and MKN74 gastric carcinoma cells (Fig. 1g–i and Extended Data Fig. 3a–e).

We next examined the roles of R9AP in EBV infection of B cells. R9AP knockout significantly decreased EBV infection of Raji Burkitt lymphoma cells, which are commonly used as B cell targets (Fig. 1j and Extended Data Fig. 3f). Moreover, EBV infection was nearly completely inhibited in Raji single-cell R9AP-knockout clones (Fig. 1k,l), and largely restored by ectopic R9AP expression (Extended Data Fig. 3g,h). Furthermore, R9AP knockout by independent single guide RNA (sgRNA) substantially reduced primary human B cell infection by EBV (Extended Data Fig. 3i).

By contrast, R9AP overexpression significantly increased EBV infection in nasopharyngeal epithelial CNE1 cells, gastric epithelial AGS cells and EBV-negative Akata Burkitt cells (Extended Data Fig. 4a–d). Together, these data indicated that R9AP supports EBV infection of both epithelial and B cells.

R9AP triggers EBV fusion

To investigate the molecular basis for R9AP support of host cell infection with EBV, we first tested whether it supports EBV binding to target cells. In contrast to CR2 overexpression in HEK-293T cells, R9AP overexpression did not significantly alter EBV binding to HEK-293T, CNE1 or EBV-negative Akata cells (Extended Data Fig. 4e,f). Moreover, R9AP depletion did not affect virus binding to HNE1 or EBV-negative Akata cells (Extended Data Fig. 4g). Nonetheless, R9AP overexpression significantly increased EBV entry into CNE1 and EBV-negative Akata cells (Extended Data Fig. 4h), whereas CRISPR depletion of R9AP reduced EBV entry into HNE1 and EBV-negative Akata cells (Extended Data Fig. 4i). Thus our data suggest that R9AP is not an important receptor for EBV attachment to B or epithelial cells.

To investigate potential downstream roles of R9AP in EBV uptake, we used a cell-based EBV fusion assay, which showed that R9AP depletion significantly reduced EBV glycoprotein-driven fusion in both HEK-293T and Daudi Burkitt B cells (Extended Data Fig. 4j,k). Overexpression of R9AP with gH, gL and gB increased HEK-293T fusion (Extended Data Fig. 4l). However, co-expression of R9AP with EBV gH/gL or gB was not sufficient to induce fusion (Extended Data Fig. 4l). These results therefore suggested that R9AP supports membrane fusion driven by EBV gH/gL and gB.

R9AP interacts with EBV gH/gL

gH/gL and gB are each critical for EBV epithelial and B cell infection. We therefore assayed interactions between R9AP and these EBV glycoproteins. We transiently expressed MYC epitope-tagged gH/gL, gH or gB together with Flag-tagged R9AP in HEK-293T cells. R9AP strongly co-immunoprecipiated with gH/gL, but only weakly with gH alone (Fig. 2a,b), in line with essential roles of gL in gH folding and trafficking[4]. No association was observed between R9AP and gB (Fig. 2a,b). Similar results were obtained using mixture of whole-cell lysates from HEK-293T cells in which R9AP or gH/gL were expressed separately (Extended Data Fig. 5a). Moreover, MYC-tagged gH and gL that was overexpressed in HEK-293T cells could be used to co-immunoprecipitate endogenous R9AP from Raji cell extracts (Fig. 2c). Consistent with this result, confocal microscopy revealed co-localization of a large fraction of Alexa Fluor 594-labelled EBV with GFP-tagged R9AP expressed in HEK-293T cells (Fig. 2d) and similar results were obtained with endogenous R9AP in HNE1 cells (Fig. 2e). Furthermore, a pull-down assay using purified recombinant proteins identified association between GST-tagged $R9AP^{1–210}$ and His-tagged gH/gL (Fig. 2f). In support of their potentially direct interaction, high-affinity binding was detected by biolayer interferometry (BLI) assay (dissociation constant (K_d) = 3.27×10^{-9} M; Fig. 2g).

Because the monoclonal antibody AMMO1 inhibits EBV infection of both epithelial cells and B cells, we examined whether its binding site on gH/gL might overlap with that of R9AP with a competition binding assay using BLI. We used the antibody CL59 as a control because it binds to gH and efficiently blocks EBV infection of epithelial cells, but only partially blocks EBV infection of B cells[23]. To quantify the competition between antibody and R9AP in binding to the gH/gL, we recorded raw antibody-binding signals with (R_c) or without (R_0) GST–R9AP. The ratio R_c/R_0 reflects the intensity of competition. A ratio close to 1.0 indicates non-competitive binding whereas ratios of less than 0.7 indicate competition. Our results showed that AMMO1 strongly competed with R9AP (R_c/R_0 = 0.39) whereas CL59 did not (R_c/R_0 = 1.02) (Fig. 2h). Furthermore, AMMO1, but neither control IgG nor CL59, prevented the interaction between gH/gL and R9AP by co-immunoprecipitation assay (Fig. 2i). Together, these results demonstrated that the interaction between R9AP and gH/gL is specific and can be inhibited by AMMO1, which suggests that this is the mechanism of AMMO1-mediated neutralization.

Gp42 inhibits interaction of gH/gL and R9AP

Given that gp42 is necessary for EBV fusion with B cells but is inhibitory for fusion with epithelial cells[14,24], we investigated its effect on the interaction between R9AP and gH/gL. Co-immunoprecipitation assays revealed that soluble gp42 inhibited the interaction only in the absence of HLA class II (HLAII) (Extended Data Fig. 5b). Furthermore, fusion assays revealed that gp42 blocked the effects of R9AP on fusion in the absence or HLAII, and promoted the effects of R9AP on viral entry in the presence of HLAII, in dose-dependent manners (Extended Data Fig. 5c). These observations may explain how gp42 inhibits EBV infection of epithelial cells and indicate that gp42–HLAII and gH/gL–R9AP co-operate to promote EBV fusion.

R9AP works together with EPHA2 and NRP1

Previous reports have shown that EPHA2 and NRP1 mediate EBV membrane fusion with and infection of epithelial cells[17–19]. To examine

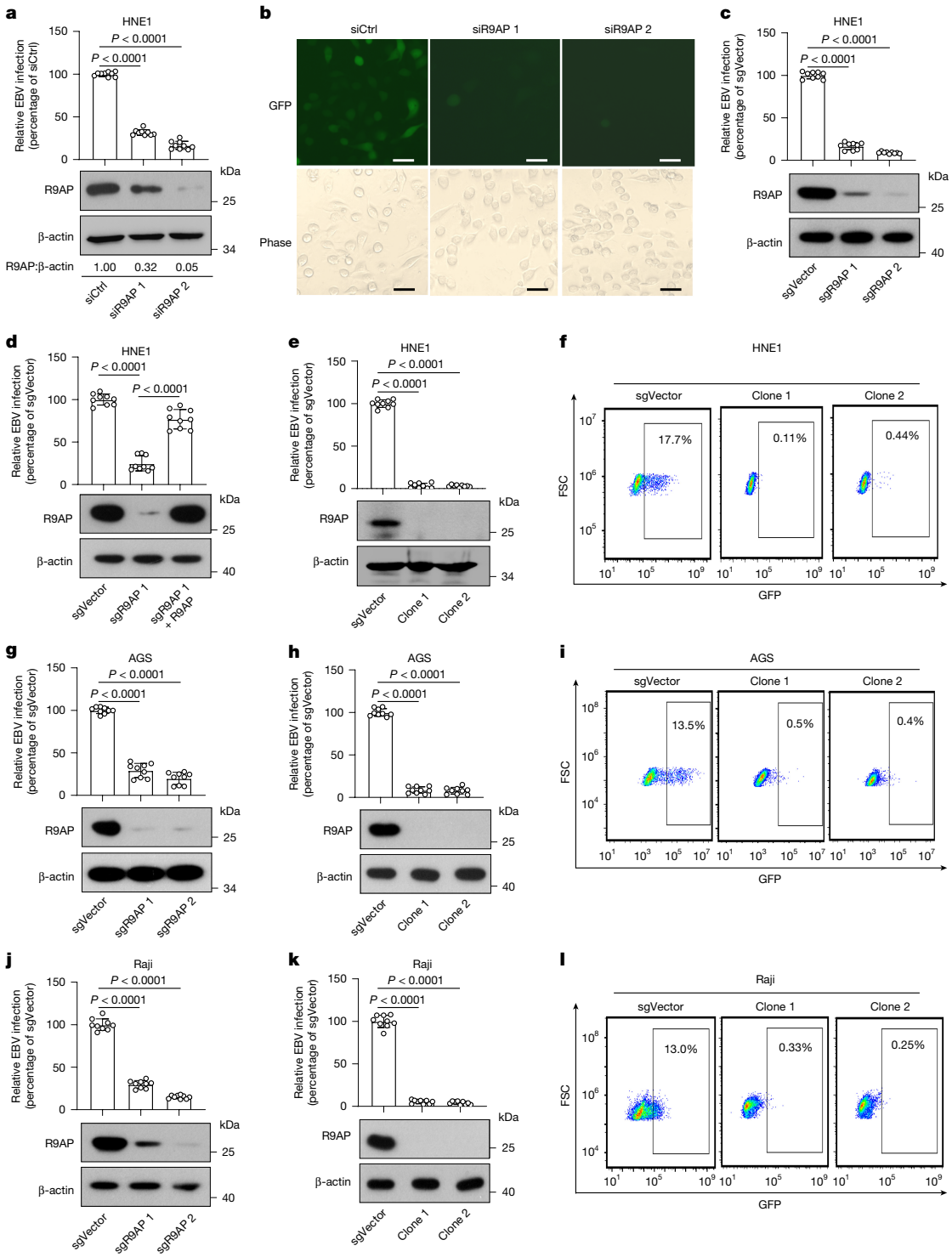

Fig. 1 | Inhibition of R9AP impairs EBV infection in epithelial and B cells. **a**,**b**, HNE1 cells were transfected with R9AP siRNA (siR9AP 1 or siR9AP 2) or control siRNA (siCtrl), then co-incubated with EBV. **a**, GFP expression was quantified by flow cytometry analysis and R9AP expression was analysed by western blot. **b**, Representative fluorescence microscopy images with EBV-positive cells shown in green. Scale bars, 100 µm. **c**,**d**, R9AP protein expression in CRISPR-edited HNE1 cells using control (sgVector) or independent R9AP sgRNA (sgR9AP 1 and sgR9AP 2) (**c**) and R9AP-reconstituted R9AP-knockout cells (**d**). EBV was added to the R9AP-knockout or reconstituted cells and EBV infection efficiency was analysed by flow cytometry. **e**,**f**, EBV infection in control and two R9AP-knockout single-cell HNE1 clones was measured by flow cytometry (**f**) and quantified (**e**, top). **e**, Bottom, R9AP protein expression in control cells and two R9AP-knockout HNE1 single-cell clones. **g**, R9AP protein expression in AGS cells expressing sgVector or R9AP sgRNA. EBV was added to AGS cells and infection efficiency was analysed by flow cytometry. **h**,**i**, EBV infection in control and two R9AP-knockout single-cell AGS clones was measured by flow cytometry (**i**) and quantified (**h**, top). **h**, Bottom, R9AP protein expression in control cells and two R9AP-knockout AGS single-cell clones. **j**, R9AP protein in control versus in R9AP-knockout Raji cells. EBV infection efficiency was analysed by flow cytometry. **k**,**l**, EBV infection in control and two R9AP-knockout single-cell Raji clones was measured by flow cytometry (**l**) and quantified (**k**, top). **k**, Bottom, R9AP protein expression in control cells and two R9AP-knockout Raji single-cell clones. Three independent experiments in triplicates ($n = 9$); data are mean ± s.e.m.; one-way ANOVA with Tukey's correction for multiple comparisons (**a**,**c**–**e**,**g**,**h**,**j**,**k**). FSC, forward scatter.

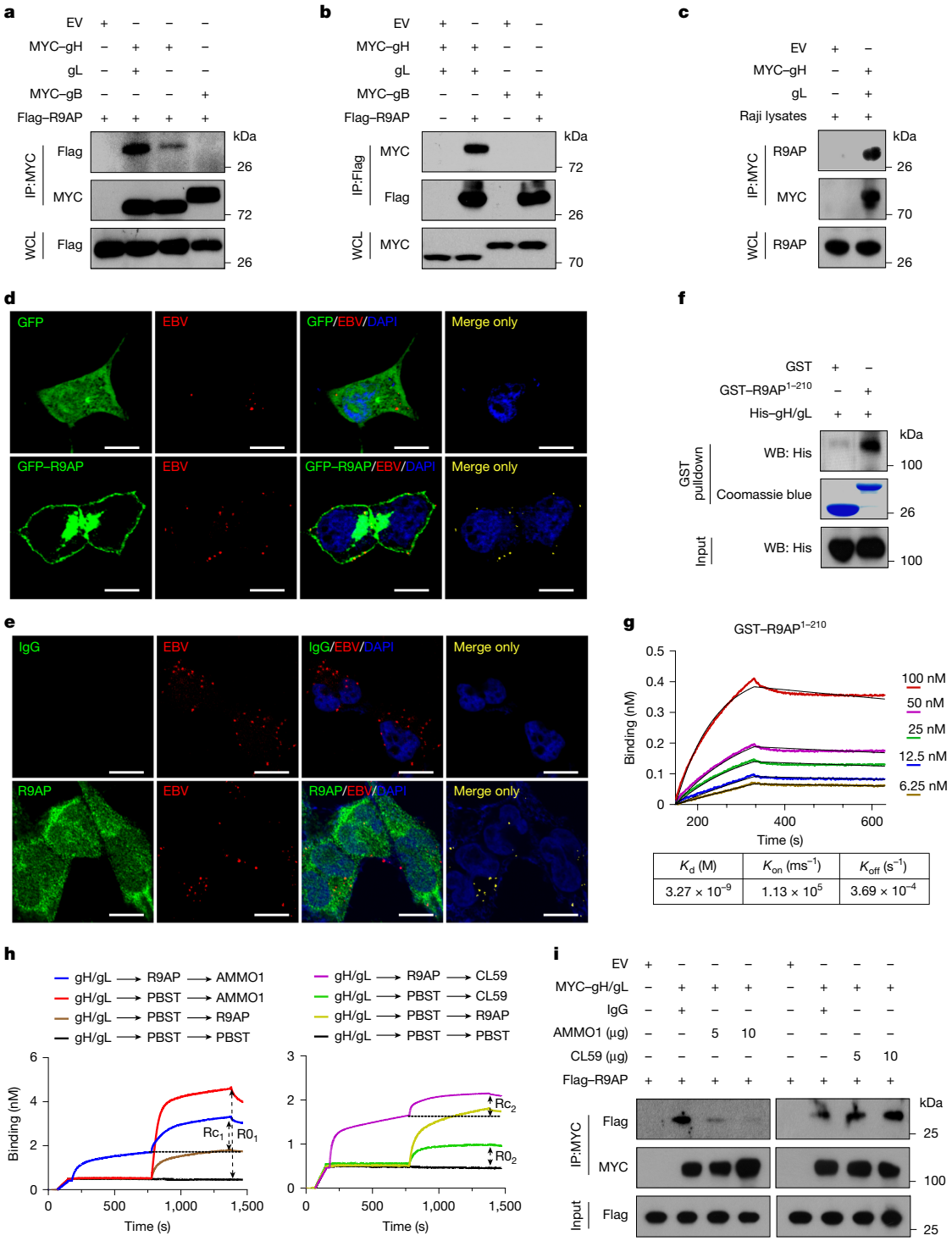

Fig. 2 | R9AP directly interacts with gH/gL. a,**b**, HEK-293T cells were co-transfected with Flag–R9AP together with empty vector (EV), MYC–gH and gL, MYC–gH or MYC–gB, lysed and immunoprecipitated (IP) with antibodies against MYC (**a**) or Flag (**b**). WCL, whole-cell lysate. **c**, HEK-293T cells were transfected with empty vector or MYC–gH and gL, lysed and incubated with Raji cell lysates. Anti-MYC immunoprecipitation was then performed with the mixed lysates, followed by western blot (WB) analysis. **d**,**e**, HEK-293T or HNE1 cells expressing GFP or GFP–R9AP were incubated with EBV at 4 °C for 1 h, then incubated at 37 °C for 30 min. GFP or GFP–R9AP (**d**) and R9AP immunofluorescence (**e**) are shown in green. EBV was detected with Alexa Fluor 594-conjugated gp350 antibody (72A1) and is shown in red. Nuclei were stained with DAPI (blue). The far right panel shows co-localization of green and red signals. Scale bars, 10 μm. **f**, His–gH/gL (containing gH amino acids 19–682 and gL amino acids 23–137) proteins were precipitated with GST or GST–R9AP$^{1–210}$ and detected by western blot. GST fusion proteins were detected by Coomassie blue staining. **g**, His–gH/gL was captured on Ni-NTA biosensors and assayed for binding to GST–R9AP$^{1–210}$. K_d, on rate (K_{on}) and off rate (K_{off}) calculated from the fit model for binding curves are shown below the graph. **h**, BLI gH/gL competition assay, with gH/gL binding to GST–R9AP$^{1–210}$ or the monoclonal antibodies AMMO1 or CL59 added in the indicated order. PBST, PBS Tween-20 vehicle. **i**, HEK-293T cells were lysed after transfection with empty vector, MYC–gH/gL or Flag–R9AP. Lysates containing MYC–gH/gL were pre-incubated with the indicated amount of antibody or IgG control and then incubated with lysates containing Flag–R9AP overnight. Mixtures were then immunoprecipitated with antibodies against MYC and western blot was performed. **a**–**f**, Data are from three independent experiments. **g**–**i**, Data are from two independent experiments.

whether R9AP and EPHA2 might jointly mediate epithelial infection, we performed rescue assays. Depletion of either EPHA2 or R9AP strongly reduced EBV fusion and infection, which were rescued by restoring expression of these proteins (Extended Data Fig. 6a–f), consistent with the model that each are important for epithelial cell uptake. Next, sequential co-immunoprecipitation assays revealed that both R9AP and EPHA2 were pulled down by immunoprecipitation of Flag-tagged gH/gL followed by MYC-tagged R9AP (Extended Data Fig. 6g). These results suggest that R9AP and EPHA2 may be present in a protein–protein complex together with gH/gL that is essential for epithelial cell infection. Overexpression of NRP1 could not rescue EBV fusion or infection of R9AP-depleted HNE1 cells (Extended Data Fig. 6h–j), indicating that R9AP and NRP1 do not have redundant roles in EBV infection.

Characterization of R9AP domains

R9AP is predicted to be a 234-residue, single-pass type IV transmembrane protein[25]. We first explored the role of the R9AP transmembrane domain (TMD; predicted to span amino acids 211–231 (ref. 26); Extended Data Fig. 7a) on EBV infection. EBV infection of HEK-293T-transfected cells was markedly decreased in cells expressing a R9AP mutant lacking the TMD ($R9AP^{1–210}$) compared with cells expressing wild-type R9AP (Fig. 3a and Extended Data Fig. 7b). These results indicated that the TMD of R9AP is critical for EBV infection, potentially owing to an obligatory role in membrane anchoring.

To further explore R9AP domains that are important for EBV infection, we constructed a series of R9AP mutants with deletions in the N-terminal region (Extended Data Fig. 7a). Deletion of the N-terminal Habc trihelical bundle (HTB) domain and linker amino acids 1–50, but not of amino acids 51–100, 101–152 or the SNARE domain 153–200, significantly impaired the ability of R9AP to support EBV infection of HEK-293T cells compared with HEK-293T cells over-expressing wild-type R9AP (Fig. 3b and Extended Data Fig. 7c). Notably, flow cytometry analysis showed similar cell surface expression levels of wild-type R9AP and R9AP(Δ1–50) (Extended Data Fig. 7d).

The N-terminal region of R9AP was previously assumed to localize intracellularly to anchor RGS9 to the disk membrane[25]. Next, we used InterPro[27] and TMHMM[28] software, confocal microscopy and biochemical analysis to characterize the subcellular localization of R9AP. Both algorithms predicted extracellular localization for the N-terminal region of R9AP (Extended Data Fig. 8a,b), which was verified by immunofluorescent staining using an anti-R9AP antibody that targets the N terminus of endogenous R9AP (Extended Data Fig. 8c). Moreover, immunofluorescent staining assays revealed that MYC–$R9AP^{1–210}$ was exlusively localized in the cytoplasm (Extended Data Fig. 8d). By contrast, MYC–R9AP was detected at the cell surface of intact HNE1 cells and was detected both in the cytoplasm and at the plasma membrane of these cells after permeabilization (Extended Data Fig. 8d). Together, these results indicated that the N terminus of R9AP could be exposed to cell surface.

Furthermore, we designed a biochemical experiment to confirm the extracellular localization of the N terminus of R9AP by introducing a PreScission protease (PSP)-recognition site (psp) between the Flag tag and full-length R9AP (Flag–psp–R9AP) or $R9AP^{1–210}$ (Flag–psp–$R9AP^{1–210}$). The Flag tag would be removed only if the PSP recognition site was presented outside of cells in the presence of PSP (Extended Data Fig. 8e). Western blotting assays revealed that PSP treatment markedly reduced the amount of Flag–psp–R9AP detected by anti-Flag but not by anti-R9AP (Extended Data Fig. 8f), indicating the removal of the N-terminal Flag tag of Flag–psp–R9AP at the extracellular surface by PSP digestion. By contrast, similar amounts of $R9AP^{1–210}$ were detected by anti-Flag or anti-R9AP antibodies in HNE1 cells expressing Flag–psp–$R9AP^{1–210}$ regardless the presence or absence of PSP, suggesting the intracellular localization of the N terminus with the PSP recognition site. Collectively, these data suggest that the N terminus of R9AP could be exposed on the cell surface.

R9AP peptide impairs EBV infection

Since the N-terminal 50 residues of R9AP support EBV infection, we next tested the effects on EBV infection of exogenous addition of a series of peptides tiling the N terminus of R9AP ($R9AP^{1–12}$, $R9AP^{13–24}$, $R9AP^{19–30}$, $R9AP^{30–41}$ and $R9AP^{35–46}$) compared with a scrambled control peptide. Flow cytometry assays revealed that $R9AP^{19–30}$ inhibited EBV infection of HNE1 epithelial and Raji B cells in a dose-dependent manner (Fig. 3c,d and Extended Data Fig. 9a,b), with a half-maximal effective concentration (EC_{50}) of 232.9 mg l^{-1} (181.2 μM) in HNE1 cells and 215.4 mg l^{-1} (167.6 μM) in Raji cells (Extended Data Fig. 9c). Notably, $R9AP^{19–30}$ also inhibited EBV infection of primary NPECs and B cells (Fig. 3e). BLI assays showed that the binding of $R9AP^{19–30}$ to gH/gL was significantly stronger than that of the scrambled control peptide (Fig. 3f). Together, these data suggest that $R9AP^{19–30}$ has an important role in support of EBV entry into epithelial and B cells in vitro.

Next, we evaluated the effect of $R9AP^{19–30}$ in EBV infection in human cord blood reconstituted B-NDG humanized mice (Extended Data Fig. 9d; see Methods for details). Quantitative PCR (qPCR) assays revealed increasing EBV DNA load in the peripheral blood four weeks after EBV inoculation as expected (Fig. 3g), but with much lower EBV copy number at six weeks post-EBV inoculation in mice treated with $R9AP^{19–30}$ mice than in mice treated with control peptide (Fig. 3h). Moreover, $R9AP^{19–30}$ treatment extended the survival of EBV-infected B-NDG mice (Fig. 3i). However, body weight did not differ between mice treated with $R9AP^{19–30}$ versus control peptide (Extended Data Fig. 9e). Human CD20-positive B cells and EBV non-coding nuclear RNAs (EBERs) were detected in the spleens of all mice (Extended Data Fig. 9f). However, the proportion of EBER-positive cells was significantly lower in mice treated with $R9AP^{19–30}$ peptide versus control peptide (Extended Data Fig. 9g). These in vivo data suggest that $R9AP^{19–30}$ offers a degree of protection from EBV infection and that targeting R9AP could be a potential strategy against EBV infection.

Anti-R9AP antibody blocks EBV infection

We produced a monoclonal antibody (5E9) against R9AP, and validated its binding affinity and specificity for R9AP using enzyme-linked immunosorbent assay (ELISA), BLI and immunoblotting (Extended Data Fig. 10a–d). 5E9 inhibited EBV infection of primary human B cells and primary NPECs (Fig. 3j,k and Extended Data Fig. 10e), Akata and Raji Burkitt cells, HNE1 nasopharyngeal carcinoma AGS gastric carcinoma cells and HEK-293T cells (Fig. 3l and Extended Data Fig. 10f–j). These results further suggest a crucial role for R9AP in EBV infection of both B cells and epithelial cells.

R9AP expression in human tissues

To characterize R9AP expression in primary human cells, we isolated epithelial and B cells from human tonsil tissues and primary B cells from peripheral blood. Reverse transcription–PCR revealed *RGS9BP* expression in both naive and memory B cells from blood and tonsil tissues, as well as in tonsil epithelial cells (Extended Data Fig. 11a). Moreover, we detected R9AP protein in peripheral blood B cells, as well as in tonsil epithelial cells, tonsil memory, naive, germinal centre and non-germinal centre B cells subsets by flow cytometry (Extended Data Fig. 11b,c). We also detected R9AP protein by immunostaining of tonsil epithelial, memory and naive B cells (Extended Data Fig. 11d,e). R9AP-positive cells were evident from lymphoid tissue germinal centre follicular areas and were detected in the mantle cell zone, as well as within basal and suprabasal stratified squamous epithelial layers obtained from the tongue and floor of the mouth (Fig. 4a and Extended Data Fig. 12a,b). It was noteworthy that the distribution of R9AP-positive cells was similar to that of CR2-positive cells (Extended Data Fig. 12a). R9AP was also weakly expressed in nasopharyngeal pseudostratified ciliated

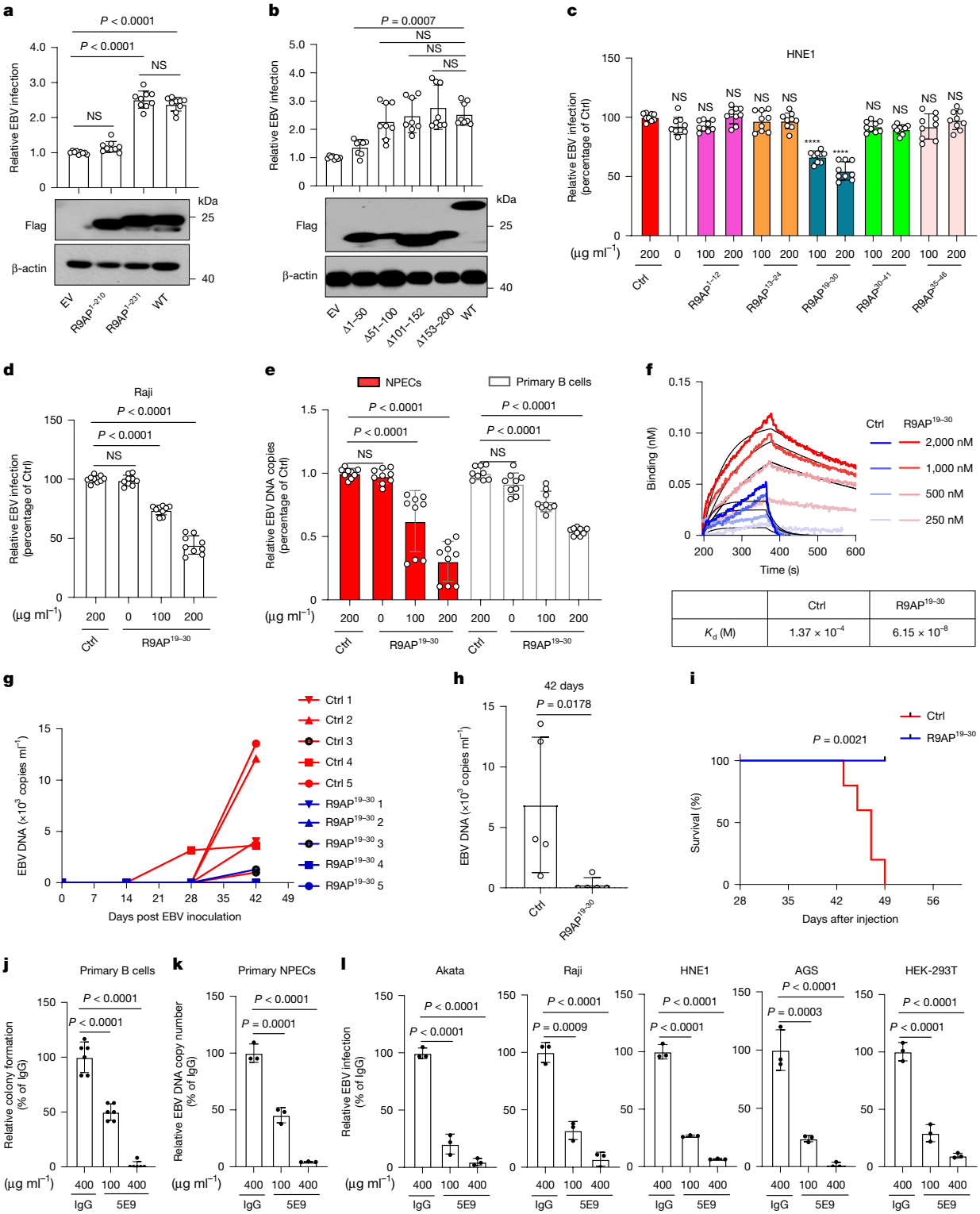

Fig. 3 | R9AP receptor function depends on its N-terminal residues and TMDs. a,**b**, Protein levels and EBV infection efficiency of ectopically expressed wild-type (WT) and truncated R9AP constructs (**a**) or WT and multiple deletions (**b**). **c**–**e**, EBV was pretreated with indicated peptide or control peptide (Ctrl) and added to HNE1 cells (**c**), Raji cells (**d**), primary NPECs or primary B cells (**e**) and EBV infection efficiency was analysed by flow cytometry (**c**,**d**) or qPCR (**e**). ****$P < 0.0001$. **f**, His–gH/gL was assayed for binding to Ctrl peptide or R9AP$^{19–30}$. $n = 2$ independent experiments. **g**–**i**, Humanized B-NDG mice were infected with EBV and treated with Ctrl peptide or R9AP$^{19–30}$ and EBV DNA copy number in peripheral blood was determined by qPCR at the indicated times (**g**,**h**). **i**, Survival curves of mice. $n = 5$ mice in each group. Data are mean ± s.e.m. (**h**). **j**–**l**, Primary B cells, NPECs, Akata, Raji, HNE1, AGS and HEK-293T cells were pretreated with R9AP monoclonal antibody (5E9) or IgG and infected with EBV, and EBV infection efficiency was analysed by counting colony formation using B cell transformation assays (**j**), qPCR (**k**) or flow cytometery (**l**). Data are mean ± s.e.m. from 3 independent experiments (**a**–**d**), primary B cells from 3 donors (**e**) performed in triplicate, $n = 9$ total replicates (**a**,**c**–**e**) or $n = 8$ total replicates (**b**). Data are mean ± s.e.m. from 1 representative of 2 (**j**) or 3 (**k**,**l**) independent experiments ($n = 6$ or 3 biological replicates). One-way ANOVA with Tukey's correction for multiple comparisons (**a**,**b**); two-way ANOVA with Sidak's correction for multiple comparisons (**c**–**e**,**j**–**l**); unpaired two-tailed *t*-test (**h**) and log-rank test (**i**). ****$P < 0.0001$. NS, not significant.

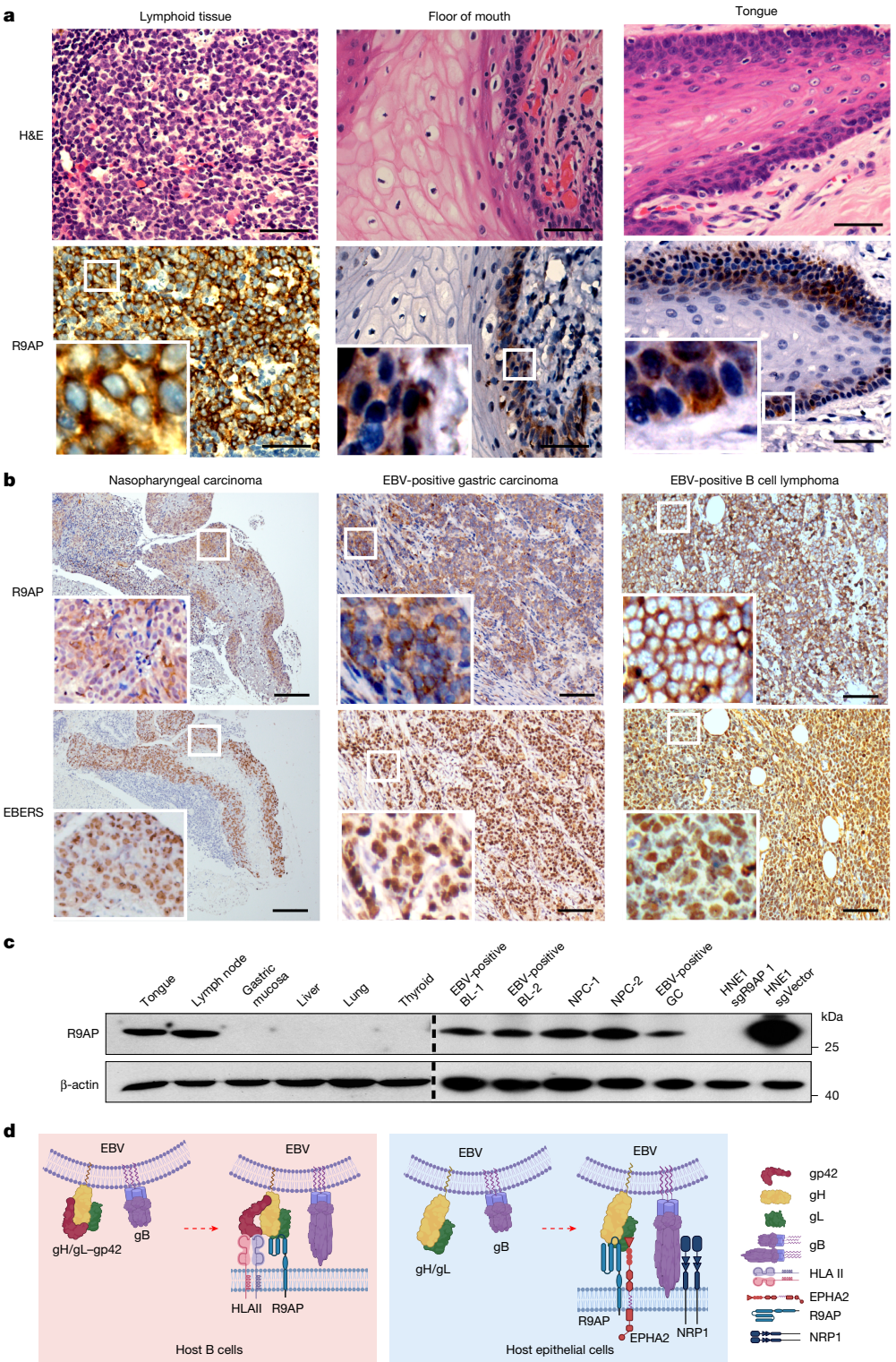

Fig. 4 | R9AP is expressed in human tissues that are susceptible to EBV infection. a, Representative immunohistochemical images of human lymphoid tissues ($n = 5$), basal layers of floor of the mouth ($n = 5$) and tongue ($n = 5$), stained with haematoxylin and eosin (H&E) (top row) or with anti-R9AP (bottom row). Inset shows 4× magnified view of the outlined region in the main image. Scale bars, 50 µm. **b**, Representative images of nasopharyngeal carcinoma ($n = 5$), gastric carcinoma ($n = 3$) and B cell lymphoma ($n = 4$) stained with anti-R9AP (top row) or EBV-encoded EBER probe (bottom row). Inset shows 4× magnified view of the outlined region in the main image. Scale bars, 100 µm. **c**, Western blot analysis of R9AP expression in human tongue, lymph node, gastric mucosa, liver, lung, thyroid, EBV-positive B cell lymphoma (BL), nasopharyngeal carcinoma (NPC) and EBV-positive gastric carcinoma (GC). HNE1 cells expressing Cas9 and sgR9AP 1 or sgVector were used as negative and positive controls, respectively. Data are representative of three independent experiments. **d**, Unified model of EBV entry. In B cells, gp42 binding to HLAII allows gH/gL to bind R9AP, which induces activation of gB-mediated viral and host membrane fusion. In epithelial cells, gH/gL simultaneously binds R9AP and EPHA2, which induces gB-mediated viral and host membrane fusion. Part **d** created in BioRender. Yang, T. (2025) https://BioRender.com/b61o826.

columnar epithelium (Extended Data Fig. 12c). We also found strong R9AP expression within dysplastic nasopharyngeal epithelium tissues (Extended Data Fig. 12c), which are more susceptible to EBV infection than normal nasopharyngeal epithelium[6,29]. By contrast, R9AP was not detected in stomach tissues (Extended Data Fig. 12c).

Moreover, we observed a similar distribution of R9AP and EBER expression in consecutive sections of EBV-positive human tumour samples, including nasopharyngeal carcinoma, gastric carcinoma and B cell lymphoma (Fig. 4b). Furthermore, western blot analysis confirmed R9AP expression in human tongue and lymph node, and in tumour samples, including EBV-positive nasopharyngeal and gastric carcinoma and B cell lymphoma, but not in normal human gastric mucosa, liver, lung or thyroid tissues (Fig. 4c). These results demonstrate that R9AP is expressed in tissues that are susceptible to EBV infection.

Discussion

Enveloped viruses enter host cells by binding to the cell surface and fusing with cell membranes to release the capsid and nucleic acid into the cytoplasm[4]. EBV infection of B cells is generally believed to require the interaction of gp42 with HLAII, which may trigger the gH/gL and gB core fusion complex, with or without an unknown host cell receptor, to achieve virus–host membrane fusion[12]. We previously identified EPHA2 and NRP1 as receptors for gH/gL or gB in EBV fusion with epithelial cells[17–19]. Our results here suggest that gp42 in the tripartite gH/gL–gp42 complex can restrict access of gH/gL to R9AP, but that gp42 interaction with its receptor HLAII allows gH/gL within the tripartite complex to then interact with R9AP to drive B cell entry (Fig. 4d). These results suggest that a gp42 conformational change after binding to HLAII might cause a further conformational change in gH/gL to expose its R9AP-binding region. Interaction of gH/gL with R9AP might further trigger a conformational change in gB to drive its membrane fusogenic activity. However, gp42 inhibits EBV fusion with epithelial cell membranes, which has been proposed as a mechanism by which epithelial cell-derived EBV, which has abundant gp42, exhibits greater B cell tropism[14]. In epithelial cell entry, EPHA2 and R9AP interact simultaneously with gH/gL, and both have crucial roles in promoting fusion (Fig. 4d). Thus, our results provide a model in which R9AP has a critical role in EBV fusion with both B and epithelial cells. This model may assist efforts to develop anti-EBV agents and vaccines that target the gH/gL–R9AP interaction.

R9AP is expressed in retinal photoreceptor cells and is localized in rod outer segment membranes, where it functions as a membrane anchor for soluble interacting partners[25]. Although R9AP expression has thus far been documented predominantly in mammalian retina, several studies have reported an important role for R9AP in bladder cancer and lung adenocarcinoma[30,31]. Our results here not only demonstrate R9AP expression in EBV-associated tumours including nasopharyngeal carcinoma, EBV-positive gastric carcinoma and EBV-positive B cell lymphoma, but also confirmed expression of *RGS9BP* or R9AP in peripheral blood, tonsillar B cells and tonsillar epithelium by RT–qPCR, immunoblot, flow cytometry and immunostaining. Several RNA-seq studies have found R9AP expression in B cells[32,33], but others have not done so[34]. Several factors may explain these inconsistencies, such as GC content bias[35], sequencing depth[36] and other variables.

We found that 8–32% of primary B cells, and nearly 23% of tonsil epithelial cells expressed R9AP. The N terminus of R9AP has previously been assumed to be present intracellularly, for example to anchor RGS9 to the disk membrane[25]. However, prompted by in silico predictions of an extracellular R9AP N terminus[27,28], we tested this with several biochemical experiments. Our experiments lead us to propose that R9AP may flip dynamically across the lipid bilayer in response to changes in membrane composition[37–40], which may also lead to an underestimation of its expression levels in flow cytometry analyses of unfixed cells that rely upon antibodies against the N terminus. Furthermore, we note that low expression of certain virus receptors in virus-susceptible host cells has been reported, such as with ACE2, which shows low or absent expression in the airway epithelium and alveoli of human lung tissues despite its crucial role in SARS-CoV-2 entry[41]. Similarly, cell surface expression of CR2 varies at the single-cell level in both Daudi and Akata cells. However, CR2-negative or low-expressing cells detected by flow cytometry are still susceptible to EBV infection, although the infection rate is lower in these cells compared with those with high CR2 expression[42]. These findings support the existence of mechanisms that dynamically regulate plasma membrane receptor expression during viral infection in vivo, and suggest that low surface expression of virus receptor can support virus infection.

We observed higher R9AP expression in tonsil memory cells than in naive B cells. We noted that EBV establishes persistence in IgD^+CD27^+ non-switched memory and IgD^-CD27^+ switched memory B cells, but apparently not in IgD^+CD27^- naive cells in vivo[43]. Given the physiology of memory cell selection, one view is that memory B cells can be preferentially infected in vivo[44]. Several studies have detected EBV-positive cells in germinal centres as well as in the interfollicular area, but not in the mantle cell zone in lymphoid tissues[45–47]. This could be explained at the level of R9AP expression and R9AP distribution in vivo, where there is evidence of expression of R9AP in the germinal centre and interfollicular area in lymphoid tissues. EBV can infect both memory and naive B cells in vitro[43,48]. However, differences in the extent to which primary B cells are susceptibility to EBV infection have been reported. Dorner et al.[48] reported that naive ($CD27^-$) and total memory ($CD27^+$) B cells from tonsils were equally susceptible to infection in short-term assays, whereas naive B cells from peripheral blood were more infectable than peripheral blood memory ($CD27^+$) preparations. Heath et al.[43] found no significant differences in virus binding, infectability or transformability between peripheral blood naive cells, non-switched memory and switched memory B cells. Thus, factors in addition to R9AP expression, which may differ in vivo versus in vitro, may account for varying susceptibility to EBV infection across B cell populations. However, since an anti-R9AP monoclonal antibody efficiently blocked peripheral blood B cell infection in vitro, our results nonetheless demonstrate that R9AP has a crucial role in B cell infection by EBV, together with additional host cell receptors that may together determine infection efficiency.

Online content

Any methods, additional references, Nature Portfolio reporting summaries, source data, extended data, supplementary information, acknowledgements, peer review information; details of author contributions and competing interests; and statements of data and code availability are available at https://doi.org/10.1038/s41586-025-09166-w.

1. Luzuriaga, K. & Sullivan, J. L. Infectious mononucleosis. *N. Engl. J. Med.* **362**, 1993–2000 (2010).
2. Bjornevik, K. et al. Longitudinal analysis reveals high prevalence of Epstein–Barr virus associated with multiple sclerosis. *Science* **375**, 296–301 (2022).
3. Shannon-Lowe, C. & Rickinson, A. The global landscape of EBV-associated tumors. *Front. Oncol.* **9**, 713 (2019).
4. Hutt-Fletcher, L. M. Epstein–Barr virus entry. *J. Virol.* **81**, 7825–7832 (2007).
5. Zhong, L. Y. et al. Research landmarks on the 60th anniversary of Epstein–Barr virus. *Sci. China Life Sci.* **68**, 354–380 (2025).
6. Young, L. S., Yap, L. F. & Murray, P. G. Epstein–Barr virus: more than 50 years old and still providing surprises. *Nat. Rev. Cancer* **16**, 789–802 (2016).
7. Nemerow, G. R., Mold, C., Schwend, V. K., Tollefson, V. & Cooper, N. R. Identification of gp350 as the viral glycoprotein mediating attachment of Epstein–Barr virus (EBV) to the EBV/C3d receptor of B cells: sequence homology of gp350 and C3 complement fragment C3d. *J. Virol.* **61**, 1416–1420 (1987).
8. Ogembo, J. G. et al. Human complement receptor type 1/CD35 is an Epstein–Barr Virus receptor. *Cell Rep.* **3**, 371–385 (2013).
9. Mullen, M. M., Haan, K. M., Longnecker, R. & Jardetzky, T. S. Structure of the Epstein–Barr virus gp42 protein bound to the MHC class II receptor HLA-DR1. *Mol. Cell* **9**, 375–385 (2002).
10. Sun, C. et al. A gB nanoparticle vaccine elicits a protective neutralizing antibody response against EBV. *Cell Host Microbe* **31**, 1882–1897.e1810 (2023).

11. Sun, C. et al. Structural basis of Epstein–Barr virus gp350 receptor recognition and neutralization. *Cell Rep.* **44**, 115168 (2025).
12. Connolly, S. A., Jackson, J. O., Jardetzky, T. S. & Longnecker, R. Fusing structure and function: a structural view of the herpesvirus entry machinery. *Nat. Rev. Microbiol.* **9**, 369–381 (2011).
13. Borza, C. M. & Hutt-Fletcher, L. M. Alternate replication in B cells and epithelial cells switches tropism of Epstein–Barr virus. *Nat. Med.* **8**, 594–599 (2002).
14. Kirschner, A. N., Omerovic, J., Popov, B., Longnecker, R. & Jardetzky, T. S. Soluble Epstein–Barr virus glycoproteins gH, gL, and gp42 form a 1:1:1 stable complex that acts like soluble gp42 in B-cell fusion but not in epithelial cell fusion. *J. Virol.* **80**, 9444–9454 (2006).
15. Yoshiyama, H., Imai, S., Shimizu, N. & Takada, K. Epstein–Barr virus infection of human gastric carcinoma cells: implication of the existence of a new virus receptor different from CD21. *J. Virol.* **71**, 5688–5691 (1997).
16. Xiong, D. et al. Nonmuscle myosin heavy chain IIA mediates Epstein–Barr virus infection of nasopharyngeal epithelial cells. *Proc. Natl Acad. Sci. USA* **112**, 11036–11041 (2015).
17. Chen, J. et al. Ephrin receptor A2 is a functional entry receptor for Epstein–Barr virus. *Nat. Microbiol.* **3**, 172–180 (2018).
18. Zhang, H. et al. Ephrin receptor A2 is an epithelial cell receptor for Epstein–Barr virus entry. *Nat. Microbiol.* **3**, 1–8 (2018).
19. Wang, H. B. et al. Neuropilin 1 is an entry factor that promotes EBV infection of nasopharyngeal epithelial cells. *Nat. Commun.* **6**, 6240 (2015).
20. Tugizov, S. M., Berline, J. W. & Palefsky, J. M. Epstein–Barr virus infection of polarized tongue and nasopharyngeal epithelial cells. *Nat. Med.* **9**, 307–314 (2003).
21. Snijder, J. et al. An antibody targeting the fusion machinery neutralizes dual-tropic infection and defines a site of vulnerability on Epstein–Barr virus. *Immunity* **48**, 799–811.e799 (2018).
22. Singh, S. et al. Neutralizing antibodies protect against oral transmission of lymphocryptovirus. *Cell Rep. Med.* **1**, 100033 (2020).
23. Sathiyamoorthy, K. et al. Inhibition of EBV-mediated membrane fusion by anti-gHgL antibodies. *Proc. Natl Acad. Sci. USA* **114**, E8703–E8710 (2017).
24. Haan, K. M., Lee, S. K. & Longnecker, R. Different functional domains in the cytoplasmic tail of glycoprotein B are involved in Epstein–Barr virus-induced membrane fusion. *Virology* **290**, 106–114 (2001).
25. Hu, G. & Wensel, T. G. R9AP, a membrane anchor for the photoreceptor GTPase accelerating protein, RGS9-1. *Proc. Natl Acad. Sci. USA* **99**, 9755–9760 (2002).
26. UniProt Consortium, T. UniProt: the universal protein knowledgebase. *Nucleic Acids Res.* **46**, 2699 (2018).
27. Mitchell, A. L. et al. InterPro in 2019: improving coverage, classification and access to protein sequence annotations. *Nucleic Acids Res.* **47**, D351–D360 (2019).
28. Krogh, A., Larsson, B., von Heijne, G. & Sonnhammer, E. L. Predicting transmembrane protein topology with a hidden Markov model: application to complete genomes. *J. Mol. Biol.* **305**, 567–580 (2001).
29. Young, L. S. & Rickinson, A. B. Epstein–Barr virus: 40 years on. *Nat. Rev. Cancer* **4**, 757–768 (2004).
30. Yang, Z. et al. Single-cell sequencing reveals variants in *ARID1A*, *GPRC5A* and *MLL2* driving self-renewal of human bladder cancer stem cells. *Eur. Urol.* **71**, 8–12 (2017).
31. Zhao, J. et al. Construction of a specific SVM classifier and identification of molecular markers for lung adenocarcinoma based on lncRNA–miRNA–mRNA network. *Onco Targets Ther.* **11**, 3129–3140 (2018).
32. Kharabi Masouleh, B. et al. Mechanistic rationale for targeting the unfolded protein response in pre-B acute lymphoblastic leukemia. *Proc. Natl Acad. Sci. USA* **111**, E2219–E2228 (2014).
33. Dombroski, B. A. et al. Gene expression and genetic variation in response to endoplasmic reticulum stress in human cells. *Am. J. Hum. Genet.* **86**, 719–729 (2010).
34. Lamontagne, R. J. et al. A multi-omics approach to Epstein–Barr virus immortalization of B-cells reveals EBNA1 chromatin pioneering activities targeting nucleotide metabolism. *PLoS Pathog.* **17**, e1009208 (2021).
35. Benjamini, Y. & Speed, T. P. Summarizing and correcting the GC content bias in high-throughput sequencing. *Nucleic Acids Res.* **40**, e72 (2012).
36. Cole, J. J. et al. Searchlight: automated bulk RNA-seq exploration and visualisation using dynamically generated R scripts. *BMC Bioinformatics* **22**, 411 (2021).
37. Dowhan, W., Vitrac, H. & Bogdanov, M. Lipid-assisted membrane protein folding and topogenesis. *Protein J.* **38**, 274–288 (2019).
38. Bogdanov, M., Xie, J., Heacock, P. & Dowhan, W. To flip or not to flip: lipid–protein charge interactions are a determinant of final membrane protein topology. *J. Cell Biol.* **182**, 925–935 (2008).
39. Vitrac, H., MacLean, D. M., Jayaraman, V., Bogdanov, M. & Dowhan, W. Dynamic membrane protein topological switching upon changes in phospholipid environment. *Proc. Natl Acad. Sci. USA* **112**, 13874–13879 (2015).
40. Woodall, N. B., Hadley, S., Yin, Y. & Bowie, J. U. Complete topology inversion can be part of normal membrane protein biogenesis. *Protein Sci.* **26**, 824–833 (2017).
41. Aguiar, J. A. et al. Gene expression and in situ protein profiling of candidate SARS-CoV-2 receptors in human airway epithelial cells and lung tissue. *Eur. Respir. J.* **56**, 2001123 (2020).
42. Speck, P. & Longnecker, R. Epstein–Barr virus (EBV) infection visualized by EGFP expression demonstrates dependence on known mediators of EBV entry. *Arch. Virol.* **144**, 1123–1137 (1999).
43. Heath, E. et al. Epstein–Barr virus infection of naive B cells in vitro frequently selects clones with mutated immunoglobulin genotypes: implications for virus biology. *PLoS Pathog.* **8**, e1002697 (2012).
44. Kuppers, R. B cells under influence: transformation of B cells by Epstein–Barr virus. *Nat. Rev. Immunol.* **3**, 801–812 (2003).
45. Roughan, J. E., Torgbor, C. & Thorley-Lawson, D. A. Germinal center B cells latently infected with Epstein–Barr virus proliferate extensively but do not increase in number. *J. Virol.* **84**, 1158–1168 (2010).
46. Mohamed, G. et al. Epstein–Barr virus, the germinal centre and the development of Hodgkin's lymphoma. *J. Gen. Virol.* **95**, 1861–1869 (2014).
47. Jamiyan, T., Nakazato, Y., Kuroda, H., Kojima, M. & Imai, Y. Characteristic histological findings of asymptomatic EBV-associated lymphoproliferative disorders in tonsils. *J. Clin. Exp. Hematop.* **58**, 122–127 (2018).
48. Dorner, M. et al. Distinct ex vivo susceptibility of B-cell subsets to Epstein–Barr virus infection according to differentiation status and tissue origin. *J. Virol.* **82**, 4400–4412 (2008).

Methods

Cell lines

Bmi1 immortalized NPECs (NPEC-Bmi1) were constructed and cultured in a keratinocyte serum-free medium (17005-075, Invitrogen) as described[16]. Human embryonic kidney 293T (HEK-293T) cells were purchased from ATCC and grown in DMEM (C11995500BT, Gibco) supplemented with 10% (vol/vol) fetal bovine serum (FBS; 10099-141C, Gibco). Raji, BJAB, Daudi, HNE1, HK1, CNE1, AGS, MKN74 and Akata cells were maintained in RPMI medium 1640 (C11875500BT, Gibco) supplemented with 5% (vol/vol) FBS. Raji, BJAB and Daudi cells were purchased from ATCC. The remaining cell lines were gifts. All cells were cultured at 37 °C in a humidified atmosphere comprising 5% CO_2 incubators without mycoplasma contamination.

Reagents

Peptides including R9AP$^{1-12}$ (MAREECKALLDG), R9AP$^{13-24}$ (LNKTTACYHHLV), R9AP$^{19-30}$ (CYHHLVLTVGGS), R9AP$^{30-41}$ (SADSQNLRQELQ), R9AP$^{35-46}$ (NLRQELQKTRQK) and scrambled control peptide (LVHYTHCGSLGV) were synthesized by Chinese Peptide. Antibodies used include: anti-R9AP for western blot and immunohistochemistry (HPA049791, Sigma-Aldrich), anti-R9AP for immunofluorescence (CSB-PA765076LA01Hu, Cusabio), anti-MYC tag (M5546, Sigma-Aldrich), anti-Flag (F3165, Sigma-Aldrich), anti-CNGA1 (DF3929, Affinity), anti-GPR1 (DF2720, Affinity), anti-SLC26A9 (SAB2105558, Sigma-Aldrich), anti-β-actin (8H10D10, 3700, Cell Signaling), anti-His tag (D3I1O, 12698, Cell Signaling), anti-EPHA2 (D4A2, 6997, Cell Signaling), anti-NRP1 (446921, AF3870, R&D Systems), CD27-AF700 (302814, BioLegend), mouse CD27-PE (LG.3A10 clone,BioLegend), EpCAM-AF594 (118222, BioLegend), CD19-AF647 (302220, BioLegend) and CD10-PE (312204, BioLegend). 72A1, CL59 and AMMO1 antibodies were generated based on the reported sequence by ourselves. PSP was a gift from S. Gao. All other reagents were obtained from Sigma-Aldrich unless indicated otherwise.

Microarray analysis

NPEC-Bmi1 MLCs and SLCs were formed and total RNA was extracted. Microarray experiments were performed by Shanghai Biochip using the Agilent Whole Human Genome Oligo Microarray 4×44K (Agilent Technologies). Differentially expressed genes were selected according to the threshold set as fold change ≥ 2.0 and a P value <0.05 according to t-test. The heat map was generated using GraphPad Prism.

Gene silencing

ON-TARGET plus SMART pool siRNAs against 72 upregulated membrane-associated genes and ON-TARGET plus siCONTROL Non-Targeting pool siRNA were purchased from GE Dharmacon (California). The two single siRNA duplexes against R9AP were as follows:

siR9AP 1: 5′-GCGAGAUGAUCGACAACAU-3′; siR9AP 2: 5′-GCAAAAGACGCGCCAGAAG-3′. siRNAs were delivered using RNAi MAX (13778150, Invitrogen) according to the kit instructions.

Generation of isogenic R9AP-knockout cell lines

The generation of HNE1, AGS, MKN74, and Raji R9AP-knockout cell lines was based on CRISPR–Cas9 gene-editing technology. The guide RNA (gRNA) sequences were 5′-CGAGTCCGCCGAGCCACCGA-3′ (sgR9AP 1) and 5′-GCTGACCGTCGGTGGCTCGG-3′ (sgR9AP 2). Oligonucleotides corresponding to the gRNA were synthesized and cloned into Cas9-expressing plasmid lentiCRISPRv2 (52961, Addgene). HNE1 cells, AGS cells, MKN74 cells and Raji cells were infected with lentivirus encoding R9AP gRNA for 6 h, and after 24 h, cells were selected with puromycin (1 μg ml^{-1}) for 3 days. Then, these selected cells were diluted to one cell per 100 μl medium and cultured in 96-well plates to obtain the single-cell-derived R9AP-knockout cell clones.

Expression of cDNA

The indicated plasmids were delivered using Lipofectamine 3000 (L3000150, Invitrogen) following the instructions in the kit. The establishment of R9AP stable expression EBV-negative Akata cells was based on the pBABE-Puro Retroviral system (RTV-001-puro, Cell BioLabs) or pHAGE-puro Lentivirus vector (#118692, Addgene).

In vitro EBV infection

Recombinant EBV encoding an GFP maker (EBfaV-GFP) was prepared from EBV-positive Akata cells[19,42]. Viral gene equivalents were determined by analysing viral supernatants, as reported previously, by qPCR[49–51]. SLCs of NPEC-Bmi1, HEK-293T, Raji, BJAB and EBV-negative Akata cells were infected with ~10–50 encapsidated EBV genomes per cell; HNE1, CNE1, AGS and MKN74 cells were infected with ~50–100 encapsidated EBV genomes per cell. The indicated cell lines were incubated with EBV for 3 h at 37 °C, and the unbound virus was discarded by washing with PBS three times. Then, cells were cultured in a fresh medium for 24 h, then quantified GFP-positive cells using flow cytometry.

Binding, entry and fusion assay

EBV binding, entry and fusion assay was performed as described[16,18,19].

Peptide blocking assay

EBV was pre-incubated at 4 °C for 2 h with the indicated peptide, diluted to 100 or 200 μg ml^{-1} in FBS-free RPMI 1640, then added to the cells. The scramble control peptide was used at 200 μg ml^{-1}. Cells were co-incubated with EBV at 37 °C for 3 h and washed 3 times with PBS. The percentages of EBV-infected HNE1 and Raji cells were determined by flow cytometry at 24 h post-infection. Primary NPECs were collected after 24 h, and primary B cells were collected after 72 h to extract DNA. EBV DNA copy number was determined by qPCR.

Protein expression and purification

GST–R9AP$^{1-210}$ was expressed in *Escherichia coli* BL21 (DE3) cells (CB105-02, Tiangen), His–gH/gL protein containing gH amino acids 19–682, gL amino acids 23–137 and His–gp42 protein containing the extracellular portion of gp42 (amino acids 34–223) were expressed in expi293F cells (A14527, Thermo Fisher). Proteins were purified as described[52,53].

Immunoprecipitation and GST pull-down assay

For co-immunoprecipitation assays, HEK-293T cells were transfected with the indicated plasmid and lysed in lysis buffer containing 1% NP-40 (N885726, Macklin), 150 mM NaCl, 2.5 mM EDTA, 20 mM HEPES pH 7.4 and protease inhibitor cocktail (5892970001, Roche). The lysates were cleared by centrifugation at 12,000 rpm, 4 °C for 10 min. The supernatants were incubated overnight with Anti-Flag M2 Gel or Anti-MYC Agarose Affinity Gel. Then, gels were washed three times with lysis buffer and subjected to western blot analysis.

To determine whether R9AP and EPHA2 could bind simultaneously to gH/gL, HEK-293T cells were transfected with MYC–R9AP and EPHA2 with Flag–gH/gL or empty vector for 36 h. Then cells were lysed and immunoprecipitated with antibodies against Flag as indicated. A portion of the sample was used as input and analysed by western blot. The remaining sample was eluted by the Flag peptide. A portion of the elution was used as input and analysed by western blot analysis. The remaining elution was re-immunoprecipitated with antibody against MYC as indicated followed by western blot analysis.

GST–R9AP$^{1-210}$ and His–gH/gL were incubated in lysis buffer overnight, washed three times with lysis buffer, and analysed by western blot for the GST pull-down assay.

HEK-293T cells were transfected with Flag–R9AP or MYC–gH/gL for the antibody competition binding assay and lysed. Cells transfected with empty vector were used as control. Lysates containing MYC–gH/gL

protein were incubated with indicated antibody overnight and then incubated with lysates containing Flag–R9AP or the control overnight. Finally, MYC–gH/gL was pulled down using Anti-MYC Agarose Affinity Gel, washed three times with lysis buffer and analysed by western blot.

For the effect of gp42 protein on the R9AP interaction with gH/gL, HEK-293T cells were co-transfected with R9AP, empty vector or Flag–HLAII, empty vector or MYC–gp42, and empty vector or MYC–gH/gL for 36 h. Cells were lysed. Then immunoprecipitated with antibody against MYC, followed by western blot analysis using Image Lab (v.5.2.1) with the indicated antibody.

Biolayer interferometry

BLI assays were performed on an Octet Red 96 instrument (18-1127, ForteBio), and the results were analysed using ForteBio data analysis software (v.8.0);. All signals were recorded at the standard frequency (5.0 Hz). For kinetic analysis, Ni-NTA biosensors (18-5101, ForteBio) were incubated in PBS with 0.05% Tween-20 for 15 min before performing the kinetic analysis. After 60 s of primary baseline, His–gH/gL protein diluted with the buffer was loaded at 0.5 μg ml^{-1} for 120 s, followed by a secondary baseline equilibration for 30 s. Then, the association of baseline-control and GST–R9AP$^{1–210}$ at a concentration gradient from 6.25 nM to 100 nM was recorded for 180 s, followed by a transition to a dissociation process for 600 s and multiple rounds regeneration with 10 mM glycine pH 1.5 (GE Healthcare). Similar procedures were performed to determine the binding affinity of R9AP peptide or control peptide to gH/gL, except for changes in association time and dissociation time to 100 s and 200 s. The raw curves were baseline-subtracted before fitting to the 1:1 binding model using the ForteBio data analysis software, after which the mean kinetic parameters (K_d, K_{on}, K_{off}) were rendered via a global fit to all binding curves.

For competition analysis, His–gH/gL protein diluted with the same buffer was loaded onto the Ni-NTA biosensor at 1 μg ml^{-1} for 180 s. After 30 s of equilibration, the primary association of GST–R9AP$^{1–210}$ or PBST was recorded until saturation for 600 s, followed by the secondary association of AMMO1 or CL59 for another 600 s. The sensors were regenerated with 10 mM glycine pH 1.5. Real-time binding was recorded during the experiment, and competitive or non-competitive behaviour was determined by the binding response presented by different association couples.

EBV fluorescence labelling

The 72A1 antibody[54] was labelled with LinKine AbFluor 594 Labeling Kit (KTL0540-50K, Abbkine) according to the manufacturer's instructions. To label EBV with AF59, the labelled antibody was incubated with EBV solution at a ratio of 1:200 at 4 °C for 2 h.

Analysis of R9AP expression in cell lines and human samples by RT–qPCR and flow cytometry

Blood peripheral blood mononuclear cells (PBMCs) were isolated using Ficoll density gradient centrifugation. Tonsil biopsies were minced, sorted with EasySep Human EpCAM Pos Slctn Kit II (17846, STEMCELL) or EasySep Hu Memory B Cell Iso Kit (17864, STEMCELL). Then sorted cells were verified by flow cytometry using Beakman Gallios, CytExpert (v.2.4.0) with anti-Human Epithelial Cell Antibody, Clone 5E11.3.1 (60147, STEMCELL) or anti-human CD19, anti-mouse/rat/human CD27 and anti-human CD10 (302220, 124209 and 312204, respectively, Biolegend).

To detect R9AP by RT–qPCR using Bio-Rad CFX Maestro 1.1, RNAs of separated cells were extracted, and reverse-transcribed and reaction systems without reverse transcriptase were used as a negative control. The mRNA level was quantified and normalized to *ACTB*.

For detection of R9AP by flow cytometry, collected tonsil epithelial cells were stained with anti-human R9AP antibody or anti-human IgG antibody (CSB-PA765076LA01Hu or CSB-PA00120E1Rb, Cusabio) and Alexa Fluor 594 anti-mouse CD326 (EpCAM) Antibody (118222 Biolegend). Blood and tonsil cells were stained with anti-human R9AP or IgG antibodies (CSB-PA765076LA01Hu or CSB-PA00120E1Rb, Cusabio) and indicated antibodies. Followed by staining with Goat anti-Rabbit IgG (H+L) Highly Cross-Adsorbed Secondary Antibody, Alexa Fluor 488 (A-11034, Invitrogen).

Immunofluorescence staining

For the co-localization assay of exogenous or endogenous R9AP with EBV using OLYMPUS FV1000, GFP-tagged R9AP or GFP transfected HEK-293T cells or HNE1 cells were co-incubated with EBV labelled with Alexa Fluor 594 for 1 h at 4 °C and 30 min at 37 °C. After removing the unbound virus, cells were fixed with 4% paraformaldehyde in PBS for 20 min at room temperature and permeabilized with 0.1% Triton X-100. Endogenous R9AP protein was stained with R9AP antibody (HPA049791) and Alexa Flour 488-labelled goat anti-rabbit IgG antibody. To determine exogenous R9AP localization, HNE1 cells were transfected with indicated plasmids, fixed and then either permeabilized with 0.1% Triton X-100 or left untreated. Then, cells were incubated with the antibody for the MYC tag (M5546, Sigma-Aldrich) and Alexa Flour 594-labelled goat anti-mouse IgG antibody. To detect the endogenous R9AP, HK1 cells were fixed and incubated with antibody targeting R9AP (HPA049791) and Alexa Flour 594-labelled goat anti-rabbit IgG antibody. For detection of endogenous R9AP in tonsil epithelial cells, memory, and naive B cells, frozen tonsil tissue sections were fixed, then incubated with R9AP antibody or anti-human IgG antibody (CSB-PA765076LA01Hu or CSB-PA00120E1Rb), anti-human CD19 and anti-mouse/rat/human CD27 Antibody (302220 and 124209, Biolegend), followed by staining with Goat anti-Rabbit IgG (H+L) antibody, Alexa Fluor 488 (A-11034, Invitrogen). Cell nuclei were counter-stained with 0.1% DAPI (D9542, Sigma-Aldrich).

PSP digestion assay

Cells were transfected with the indicated plasmids for 24 h and fixed in 4% paraformaldehyde. Then, 10 μg PSP was diluted in 500 μl PBS and incubated with the fixed cells at 4 °C for 8 h. The treated cells were washed three times with PBS and collected for western blot analysis.

R9AP monoclonal antibody screening with rabbit immunization

Two three-month-old New Zealand white male rabbits (Genescript) were immunized intramuscularly with GST–R9AP$^{1–210}$ mixed with an equal volume of Freund's complete adjuvant four times at two-week intervals to establish the humoral response to R9AP. To determine the R9AP-specific antibody titre, PreScission protease (Beyotime) was added to GST–R9AP$^{1–210}$ to remove the GST tag. Post-immunization blood was collected to confirm the seropositive level for R9AP. Then, rabbits were euthanized and the spleens were collected to collect PBMCs.

To isolate the R9AP-specific B cells, PBMCs were dyed with reagents and antibodies for sorting, including anti-rabbit IgG-AF488 (Abcam) and R9AP labelled with AF594. IgG$^+$R9AP$^+$ B cells were sorted using a BD Rhapsody cell sorter into 96-well plates containing precoated 293T-rCD40L as feeder cells, 20 ng ml^{-1} rabbit IL-2 (Beyotime), and 35 ng ml^{-1} human IL-21 (Sigma). Isolated B cells were observed for viability and cultured for seven days, and the supernatants of each well were collected for ELISA. If the endpoint ELISA titre for R9AP was greater than 512,000, the B cells from that well would be collected for further clonal sequencing.

To perform B cell clonal sequencing, B cell RNA was extracted, and cDNA was synthesized using Superscript III reverse transcriptase (Invitrogen). Antibody variable regions of heavy and light chains were amplified via nested PCR with GXL polymerase (Takara). The first PCR used gene-specific primers, while the second employed primers overlapping the leader sequence (5′) and CH1 or Cκ regions (3′). PCR products were cloned into pcDNA3.1 vectors containing rabbit constant regions for antibody production.

Antibody blocking assay

Primary B cells, NPECs, Akata, Raji, HNE1, AGS and HEK-293T cells were pretreated with anti-R9AP monoclonal antibody (5E9), then infected with EBV. EBV infection efficiency was analysed by counting colony formation using B cell transformation assays and calculating EBERs-positive cells by in situ hybridization (ISH) in primary B cells, by calculating the copy number of EBV DNA using qPCR in NPECs, or by flow cytometry in Akata, Raji, HNE1, AGS and HEK-293T cells.

In vivo EBV infection of humanized mice

Ten four- to five-week-old female immunodeficient NOD/SCID gamma (NDG) mice were purchased from Biocytogen and randomized, divided into two groups. Human cord blood was obtained from Guangzhou Women and Children's Medical Center (China). Human cord blood mononuclear cells were separated, and then 1×10^7 cells were injected intraperitoneally into 4 to 5-week-old B-NDG mice. Oethicn the same day, mice were injected through the tail vein with indicated peptide at 20 mg kg^{-1} of body weight and 30,000 encapsidated EBV genomes. Then, the mice were injected intraperitoneally with indicated peptide at 20 mg kg^{-1} of body weight on days −3, −7, and −14 and injected intraperitoneally with 50 μg OKT3 (B104, Nobimpex) on day −7. Blood was collected from the mice to extract DNA on days- 0, −14, −28 and −42. To quantify the EBV DNA copy number in mouse blood, qPCR was used to detect the BamHI-W fragment of the EBV genome using the primers 5′-CCCAACACTCCACCACACC-3′ and 5′-TCTTAGGAGCTGTCCGAGGG-3′.

Analysis of R9AP and CR2 expression by immunohistochemistry and EBER expression by ISH

Human tissues from the tongue, the floor of the mouth, lymphoid tissue, nasopharyngeal carcinoma, gastric carcinoma and B cell lymphoma were obtained from patients admitted to the Sun Yat-sen University Cancer Center. To detect R9AP and CR2 by immunohistochemistry, the antibodies against human R9AP (HPA049791, Sigma-Aldrich, diluted 1:50) and CR2 (EP64, ZSGB-Bio, diluted 1:200) were used. EBERs were detected using the ISH detection Kit (ISH-7001, ZSGB-Bio).

Analysis of the spleen of EBV-infected mice

Mice were euthanized at seven weeks. The spleens of all the mice were fixed in formalin to examine if the animals had persistent EBV infection using H&E and immunohistochemistry with antibodies against human CD20, and detection of EBERs using the ISH detection Kit. The results were independently evaluated by three pathologists, who were blinded to the status of the samples. The expression of human CD20 and EBERs was evaluated by counting 3 representative high-power fields (×40 objective) per sample, with approximately 100 cells per field.

Plasmids

cDNA fragments encoding R9AP, SLC26A9, CNGA1, $R9AP^{1–210}$, N-terminal plus TMD of R9AP (1–231), R9AP deletion mutants (Δ1–50, Δ51–100, Δ101–152 and Δ153–200), the sequence encoding the PSP recognition site and full-length sequence of R9AP (psp–R9AP) or PSP site and N-terminal amino acids 1 to 210 of R9AP (psp–$R9AP^{1–210}$), the sequences of gL (amino acids 23–137, M81 strain) and gH ectodomain (amino acids 19–679, M81 strain) connected by a linker (GGGGS)×3 were individually cloned into PCDNA3.1 (+) vector (V79020, Invitrogen); for EBV infection of EBV-negative Akata cells, the cDNA fragment encoding R9AP was cloned into the pBABE-Puro retroviral vector (RTV-001-puro, Cell Biolabs) or pHAGE-puro lentivirus vector (#118692, Addgene); for immunofluorescence staining in HNE1 cells or immunoprecipitation assay, the cDNA of full-length of R9AP, $R9AP^{1–210}$, MYC–gH, gL or MYC–gB was cloned into the pCDNA6 vector; for the GST pull-down assay, the sequence encoding $R9AP^{1–210}$ was cloned into the pGEX6p-1-GST vector; for the cell-based fusion assay, expression plasmids for pCAG-T7, pT7EMC-Luc, gB, gH or gL were used.

RT–qPCR

Total RNA was extracted using TRIzol reagent. RNA was reverse-transcribed using the RNA Reverse Transcription System (A5001, Promega). The mRNA level was quantified using the LightCycler 480 SYBR Green I Master mix (04887352001, Roche). All the gene expression data were normalized to *ACTB*. Primers were as follows: *CNGA1*: 5′-AAGGGAGGACCATCACAGA-3′ and 5′-TTCTGGTTCCTGGTCCTTA-3′; *GPR1*: 5′-TCTTATCTCATCGGCATCG-3′ and 5′-GCTTCGCTTCTTCACCTT −3′; *SLC26A9*: 5′-CAACAAGCACGGCTACGAC-3′ and 5′-TTGAGGGAGTTCTTGAGATTGA-3; *R9AP*: 5′-ATGAAGAGCGTTCGTGCCG-3′ and 5′-GCACGCAGTCGTCTTGTTGAG-3′; *EBER1*: 5′-GCCGAATACCCTTCTCCCA-3′ and 5′-TGCCCTAGTGGTTTCGGACA-3′; *EBNA1*: 5′-GTAGGGGATGCCGATTATTTTG-3′ and 5′-CTCCTTGACCACGATGCTTTC-3′; *BZLF1*: 5′-CCCAGTCTCAGACATAACCC-3′ and 5′- CAGGCTGTGGAGCACCAATG-3′; *BXLF2*: 5′- TCGATTGGGCTGGTCTGAG-3′ and 5′-TTAACCTCGCTAAGGCTGGC-3′.

Statistical analyses

The results represent the mean or mean ± s.e.m. from two or three independent experiments or the indicated number of biological replicates. Statistical analyses were performed using GraphPad Prism (GraphPad Software).

Ethical standards

Written informed consent forms were signed by all the donors and patients. The utilization of human samples was approved by the institutional review board of each institution taking part in the project. Human cord blood was obtained from Guangzhou Women and Children's Medical Center (China), approved by the Committee on the Ethics of Guangzhou Women and Children's Medical Center. Human tissues including lymphoid tissues, floor of mouth, tongue, lymph node, liver, lung, thyroid, blood, tonsil, nasopharynx epithelium, gastric mucosa and tumour tissues were collected from Sun Yat-sen University Cancer Center, approved by the Committee on the Ethics of Sun Yat-sen University Cancer Center. All animal experiments with infectious EBV were performed in the animal biosafety level 2 facilities at Sun Yat-sen University Zhongshan School of Medicine, approved by the Committee on the Ethics of Animal Experiments of Sun Yat-sen University. The animal studies were carried out according to the recommendations promulgated in the Guide for the Care and Use of Laboratory Animals of the Ministry of Science and Technology of the People's Republic of China.

Reporting summary

Further information on research design is available in the Nature Portfolio Reporting Summary linked to this article.

Data availability

There are no restrictions on data availability in this manuscript. All data are available in the main text or extended data. The uncropped western blot images are shown in the Supplementary information. Raw data for animal-related experiments in main and extended figures are provided as source data. Microarray data presented in this study are available at the NCBI Gene Expression Omnibus (GEO) repository under accession GSE159958. The key raw data of all the functional experiments of the main figures in this work has been deposited onto the Research Data Deposit public platform (https://www.researchdata.org.cn) with the approval number RDDB2020001025. All other data are available from the corresponding author on reasonable request.

49. Tsai, M. H. et al. Spontaneous lytic replication and epitheliotropism define an Epstein–Barr virus strain found in carcinomas. *Cell Rep.* **5**, 458–470 (2013).
50. Feederle, R. et al. Epstein–Barr virus BNRF1 protein allows efficient transfer from the endosomal compartment to the nucleus of primary B lymphocytes. *J. Virol.* **80**, 9435–9443 (2006).
51. Hung, C. H. et al. Regulation of autophagic activation by Rta of Epstein–Barr virus via the extracellular signal-regulated kinase pathway. *J. Virol.* **88**, 12133–12145 (2014).
52. Kang, Y. F. et al. Rapid development of SARS-CoV-2 spike protein receptor-binding domain self-assembled nanoparticle vaccine candidates. *ACS Nano* **15**, 2738–2752 (2021).
53. Sun, C. et al. Parallel profiling of antigenicity alteration and immune escape of SARS-CoV-2 Omicron and other variants. *Signal Transduct. Target. Ther.* **7**, 42 (2022).
54. Janz, A. et al. Infectious Epstein–Barr virus lacking major glycoprotein BLLF1 (gp350/220) demonstrates the existence of additional viral ligands. *J. Virol.* **74**, 10142–10152 (2000).

Acknowledgements The authors thank B. Gewurz for providing constructive suggestions on experiments and manuscript editing, M. Masucci for providing the Akata cell line, Q.-T. Liu for providing the CNE1 cell line, S.-W. Tsao for providing the HNE1 and HK1 cell lines, Q. Tao for providing the AGS cell line, X. Rui-Hua for providing the MKN74 cell line, J.-H. Han for providing the *SLC26A9* cDNA, R. Longnecker and P. G. Spear for providing plasmids pCAG-T7 and pT7EMC-Luc and CL59 antibody, W. Hammerschmidt for providing plasmid p2670, and Y.-H. Huang and Y. Zhang for pathological evaluation of immunostaining and EBER ISH of human and mouse samples. This manuscript was edited by Life Science Editors. This work was supported by the National Key Research and Development Program of China (2022YFC3400900 to M.-S.Z.), the National Natural Science Foundation of China (82030046 to M.-S.Z., U24A20743 to M.-S.Z., 32441094 to M.-S.Z. and U22A20322 to Q.Z.), the Program for Guangdong Introducing Innovative and Enterpreneurial Teams (2019BT02Y198 to M.-S.Z.), Guangdong Science and Technology Department (2020B1212030004 to M.-S.Z.), Sun Yat-sen University Talent Program (22yklj08 to Q.Z.), Cancer Innovative Research Program of Sun Yat-sen University Cancer Center (CIRP-SYSUCC-0006 to M.-S.Z.) and Young Talents Program of Sun Yat-sen University Cancer Center (YTP-SYSUCC-0090 to Q.Z.).

Author contributions M.-S.Z. and Q.Z. conceived and designed the experiments, provided supervision and wrote the manuscript. Yan Li performed and analysed the key experiments including siRNA screening, immunoprecipitation and GST pull-down assay, peptide blocking assay, analysis of R9AP expression in cell lines and human samples, PSP digestion assay, in vivo EBV infection of humanized mice and wrote the manuscript. H.Z. detected EBV infection, binding, entry and fusion in R9AP-knockout and overexpressed cell lines. C.S. performed the BLI and EBV fluorescence labelling assay, and generated R9AP monoclonal antibody. X.-D.D. purified the proteins and performed the in vivo EBV infection of humanized mice. C.X., Y.-T.L., R.-B.L. and X.-W.K. performed R9AP monoclonal antibody generation and antibody blocking assay. Z.-L.H. performed immunofluorescence staining and immunoprecipitation. X.-Y.M., D.-L.D., Q.-Y.Z., Y.-C.L., Ying Li, S.-X.L., L.Y., P.H., S.G., A.T.M., B.Z., E.R., Y.-P.T., J.-Y.Y. and Y.-X.Z. provided constructive suggestions or materials for this work. P.-H.Z., J.-X.B., B.Z. and A.T.M. helped revise the manuscript.

Competing interests Patent applications related to the R9AP monoclonal antibody 5E9 have been submitted to the China National Intellectual Property Administration (patent application number 2024119195522; M.-S.Z., C.S. and C.X. are named inventors). The other authors declare no competing interests.

Additional information

Supplementary information The online version contains supplementary material available at https://doi.org/10.1038/s41586-025-09166-w.

Correspondence and requests for materials should be addressed to Qian Zhong or Mu-Sheng Zeng.

Peer review information *Nature* thanks the anonymous reviewer(s) for their contribution to the peer review of this work. Peer review reports are available.

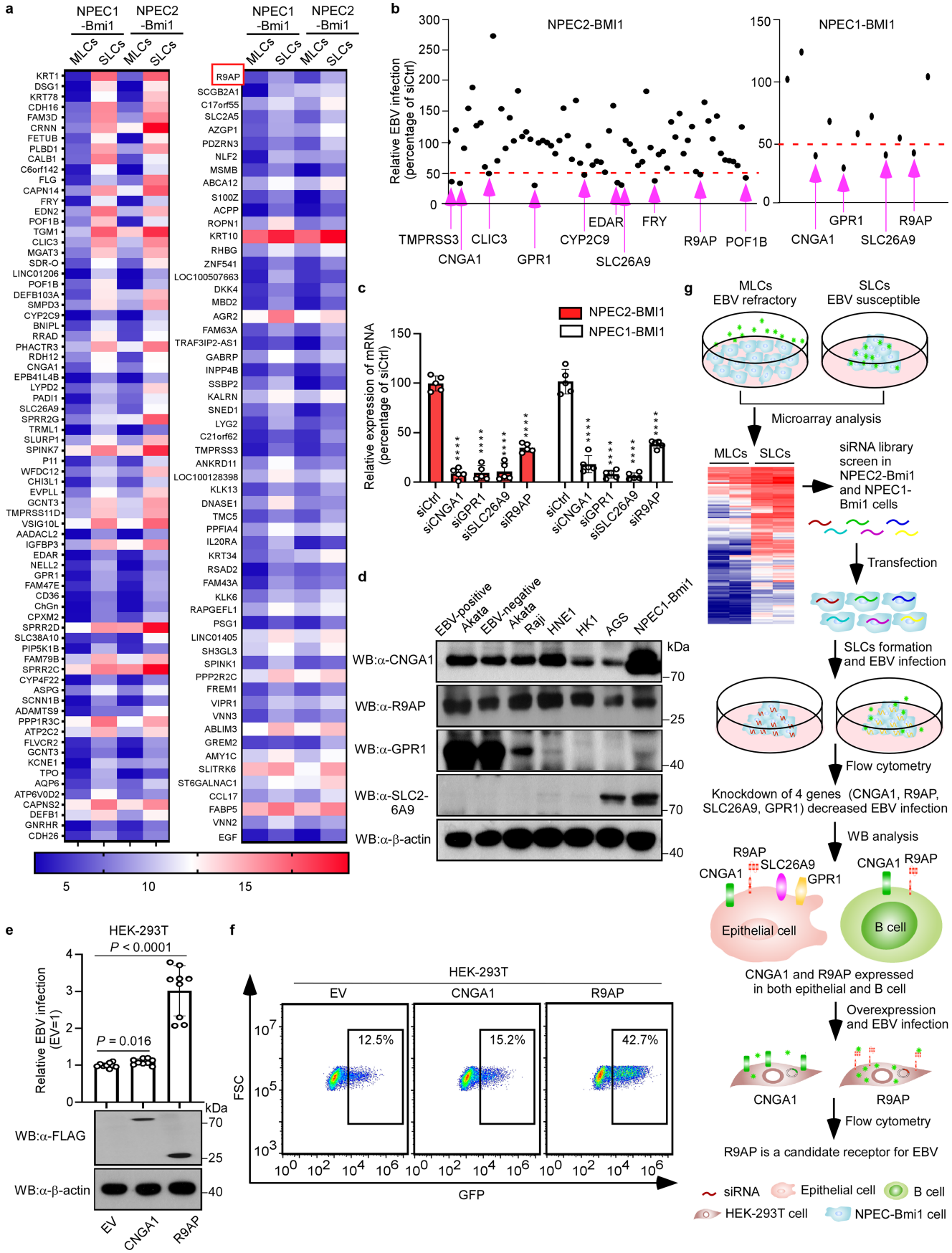

Extended Data Fig. 1 | See next page for caption.

Extended Data Fig. 1 | Screening identifies R9AP as a potential EBV receptor. a, Heatmap of genes in SLCs compared to MLCs of NPEC1-Bmi1 and NPEC2-Bmi1 cells. **b**, siRNA screening. Relative EBV infection efficiency was determined by flow cytometry. 72 siRNA pools were screened in NPEC2-Bmi1 SLCs first, and 10 siRNA pools were selected and re-screened in NPEC1- Bmi1 SLCs. Arrows indicated genes whose knockdown reduced EBV infection efficiency by more than 50% compared to the siCtrl. The dotted pink line indicated 50% of relative EBV infected cells in siCtrl transfected SLCs. Data are mean (n = 2 biological replicates). **c**, RT-qPCR was used to detect knockdown efficiency of indicated siRNA. Results were quantified relative to the housekeeping gene beta-actin (ACTB). Two independent experiments in either triplicate or duplicate (n = 5) and mean and S.E.M. of those n = 5 were used. (****$P < 0.0001$) **d**, WB analysis of the endogenous CNGA1, R9AP, GPR1, and SLC26A9 in indicated EBV susceptible cells. Data are representative of two independent experiments. **e, f**, EBV infection efficiencies, and ectopic R9AP, CNGA1 protein level of HEK-293T cells after being transfected with CNGA1, R9AP, or EV (e). Three independent experiments in triplicates (n = 9) and the mean and S.E.M. of those n = 9 were used. The percentage of EBV-infected cells was shown (f), data are representative of three independent experiments. **g**, Schematic summary of screening. Microarray was used to analyze gene expression in NPECs-Bmi1 SLCs compared to MLCs. A siRNA library targeting upregulated transmembrane associated genes in SLCs was transfected into NPECs-Bmi1. Knocking down of CNGA1, R9AP, SLC26A9, or GPR1 reduced EBV infection more than 50%, while only CNGA1 and R9AP were expressed in all indicated cell lines by WB. Finally, ectopic expressing R9AP but not CNGA1 enhanced EBV infection in HEK-293T cells. One-way ANOVA was carried out with Tukey's correction for multiple comparisons (c, e).

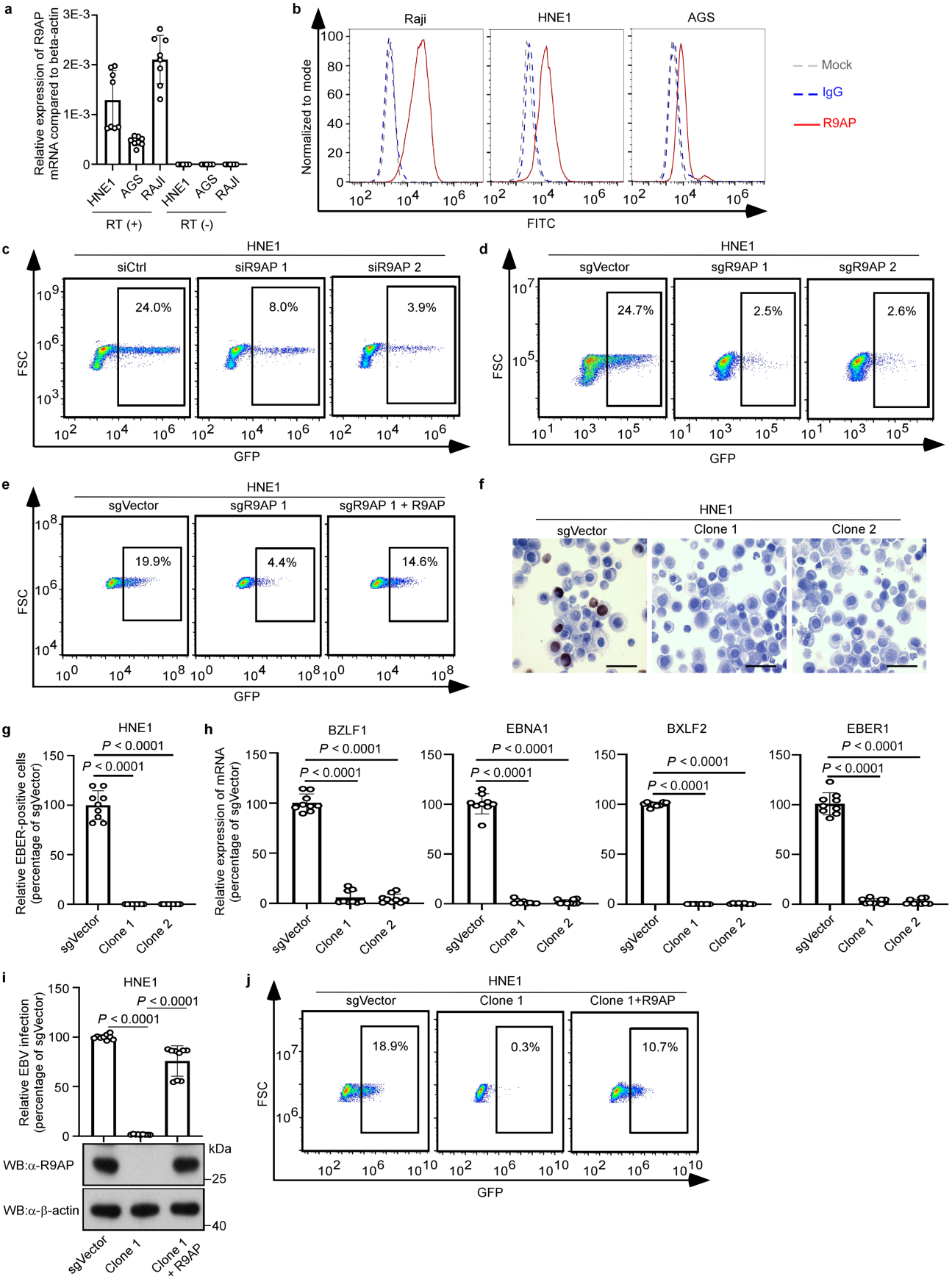

Extended Data Fig. 2 | See next page for caption.

Extended Data Fig. 2 | R9AP mediates EBV infection in nasopharyngeal epithelial cells. a, RT-qPCR was used to quantify the mRNA level of R9AP in HNE1, AGS, and Raji cells. The mRNA without reverse transcription was used as a negative control. Three independent experiments in either triplicate or duplicate (n = 8) and mean and S.E.M. of those n = 8 were used. **b**, Raji, HNE1, and AGS cells were stained with antibodies against R9AP and analyzed by flow cytometry. **c**, HNE1 cells were transfected with R9AP siRNAs (siR9AP 1 or siR9AP 2) or siCtrl, then infected with EBV, and the percentage of infected cells was determined using flow cytometry. **d, e**, HNE1 cells were knockout of R9AP using sgR9AP 1 and sgR9AP 2 (d). Then R9AP knockout cells were reconstituted with an R9AP expression vector (sgR9AP 1 +R9AP) (e). EBV was added to the R9AP knockout and reconstituted HNE1 cells, and EBV infection efficiency was analyzed by flow cytometry. **f, g**, Representative images of R9AP knockout HNE1 single-cell clones or sgVector HNE1 cells infected with EBV then hybridized with an EBV EBERs probe (f). Scale bar=50 μm. The proportion of EBERs-positive cells was independently evaluated by three pathologists (g). **h**, Single-cell clones of R9AP knockout HNE1 cells were infected with EBV and analyzed by RT-qPCR to quantify the mRNA level of indicated EBV genes. **i, j**, The R9AP protein in R9AP knockout single-cell clone 1 HNE1 cells without or with reconstitution with R9AP (i). EBV was added to these cells, and the EBV infection efficiency was analyzed by flow cytometry (j) and quantified (i). Data are representative of three independent experiments (b-f, j). Three independent experiments by three individual evaluation (n = 9; g) or in triplicates (n = 9; h, i) and mean and S.E.M. of those n = 9 were used, and one-way ANOVA was carried out with Tukey's correction for multiple comparisons (g-i).

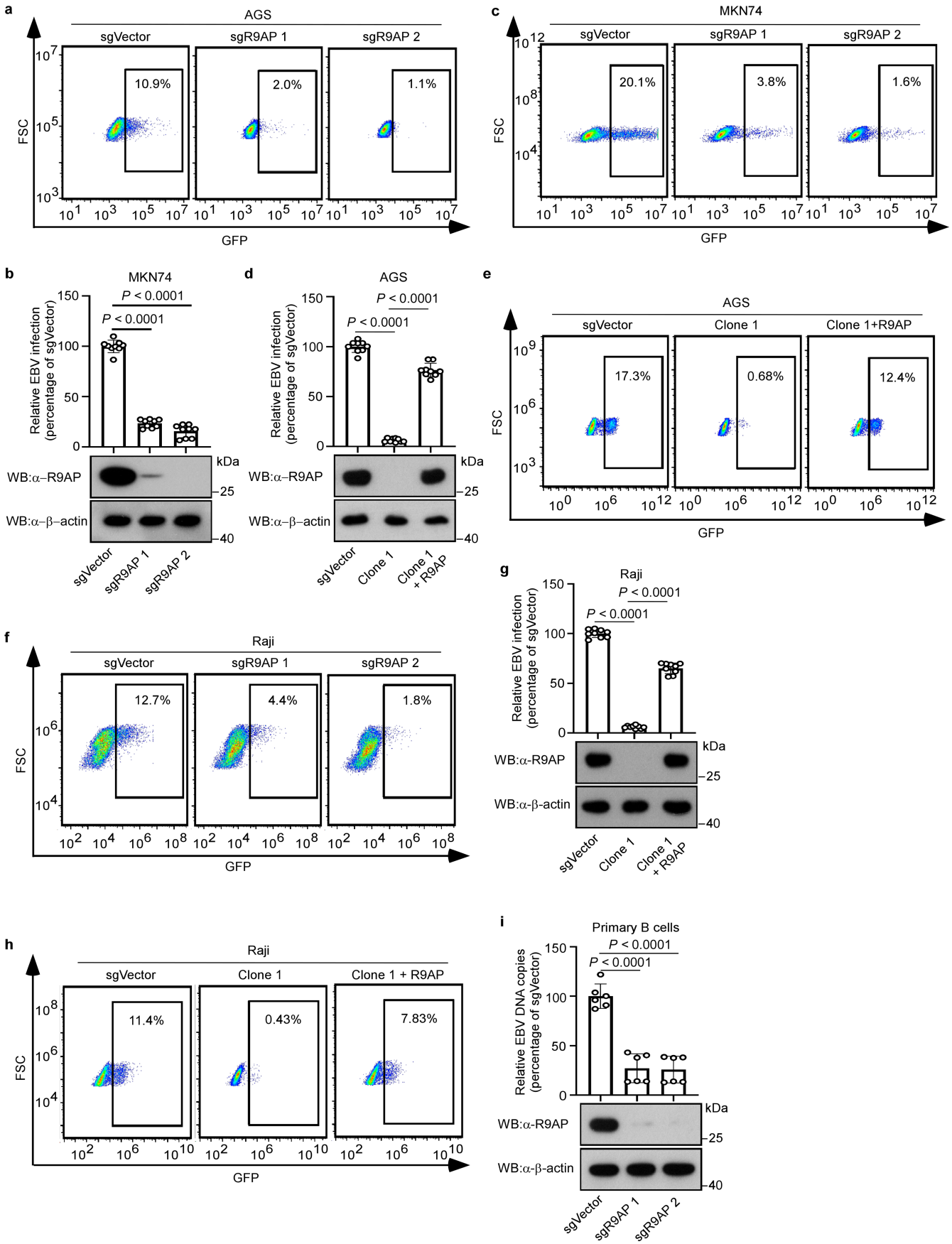

Extended Data Fig. 3 | See next page for caption.

Extended Data Fig. 3 | R9AP mediates EBV infection in gastric epithelial and B cells. a, EBV infection was determined in R9AP knockout AGS cells using flow cytometry. **b, c**, The R9AP protein in MKN74 cells knockout of R9AP using sgR9AP 1 and sgR9AP 2 (b). EBV infection was determined using flow cytometry (c), and the quantification data was shown in (b). **d, e**, The R9AP protein level in R9AP knockout single-cell clone 1 AGS cells without or with reconstitution with R9AP (d). EBV was added to these cells, and the EBV infection efficiency was analyzed by flow cytometry (e) and quantified (d). **f**, EBV infection was determined in R9AP knockout Raji cells using flow cytometry. **g, h**, The R9AP protein level in R9AP knockout single-cell clone 1 Raji cells without or with reconstitution with R9AP (g). EBV was added to these cells, and the EBV infection efficiency was analyzed by flow cytometry (h) and quantified (g). **i**, sgVector, sgR9AP 1, or sgR9AP 2 was delivered into primary B cells by a lentivirus package system. The R9AP protein level was analyzed by WB. EBV infection was analyzed by qPCR. Three independent experiments in triplicates (n = 9) and mean and S.E.M. of those n = 9 were used (b, d, g), Two independent experiments from two donors' primary B cells experiments in triplicate (n = 6) and mean and S.E.M. of those n = 6 were used (i). One-way ANOVA was carried out with Tukey's correction for multiple comparisons (b, d, g, i). Data are representative of three independent experiments (a, c, e, f, h).

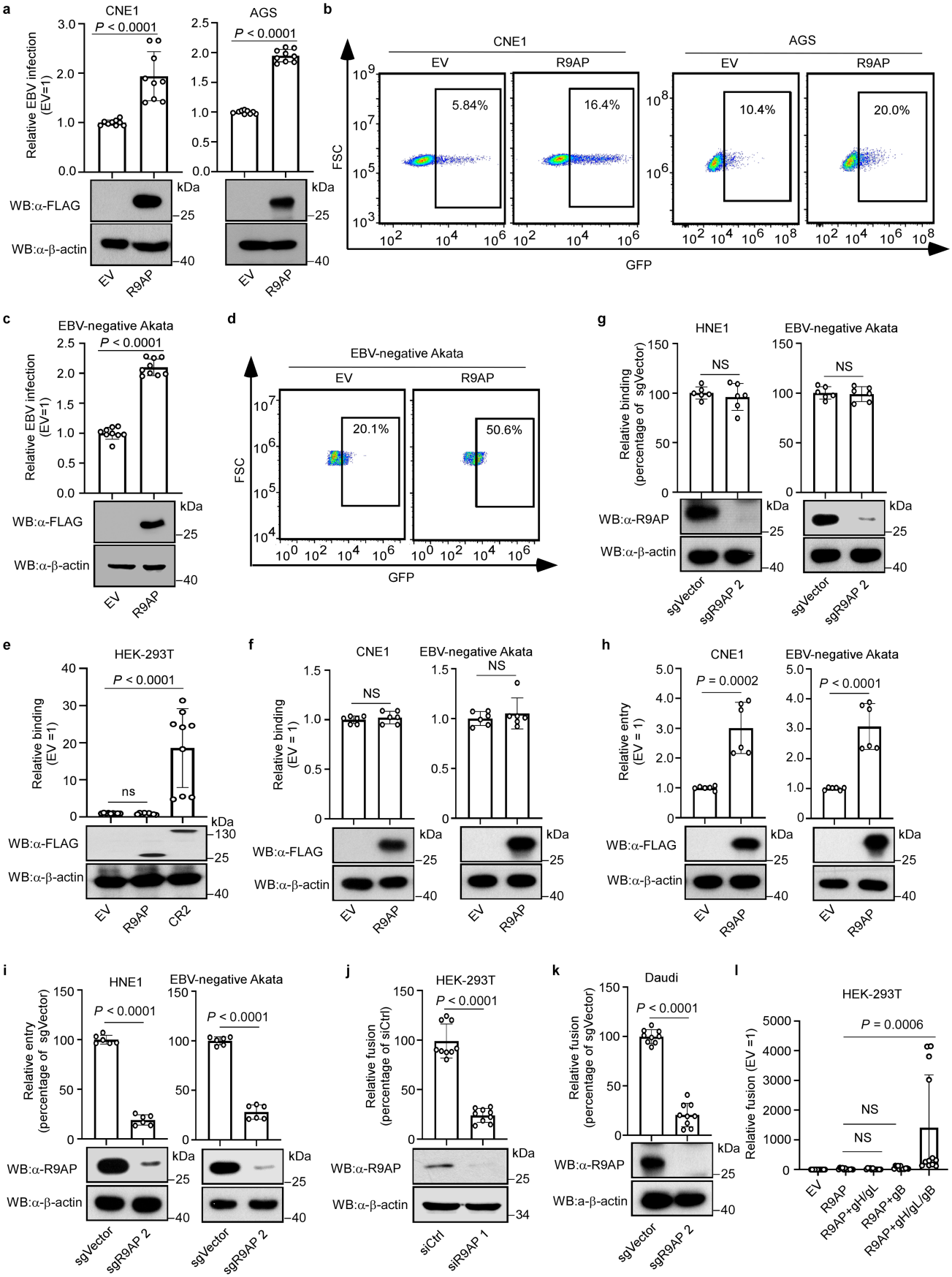

Extended Data Fig. 4 | See next page for caption.

Extended Data Fig. 4 | R9AP mediates EBV entry and fusion. a-d, Ectopic R9AP protein and EBV infection efficiency in CNE1 and AGS cells (a, b) or EBV-negative Akata cells (c, d). **e**, EBV binding in R9AP, CR2, or EV transiently transfected HEK-293T cells. **f, g**, EBV binding in R9AP or EV transiently transfected CNE1 cells or stably delivered EBV-negative Akata cells (f), in R9AP knockout HNE1 cells and EBV-negative Akata cells (g). **h, i**, EBV entry in R9AP or EV transiently transfected CNE1 cells or stably delivered EBV-negative Akata cells (h), in R9AP knockout HNE1 cells or EBV-negative Akata cells (i). **j-l**, Cell-based EBV fusion assay by co-culture of R9AP knockdown HEK-293T cells and HEK-293T cells transfected with gB and gH/gL (j), by co-culture of R9AP knockout Daudi cells, HEK-293T cells transfected with gB and gH/gL and His-gp42 protein at 0.5 μg/mL (k), by co-culture of R9AP overexpressed HEK-293T and HEK-293T cells transfected with gB, gH/gL, or gH/gL/gB (l). Three independent experiments in triplicates (n = 9) and mean and S.E.M. of those n = 9 were used (a, c, j, k, e), two independent experiments in triplicates (n = 6) and mean and S.E.M. of those n = 6 were used (f-i), or three independent experiments in quadruplicates (n = 12) and mean and S.E.M. of those n = 12 were used (l). Two-tailed unpaired Student's *t*-test (a, c, f-k), one-way ANOVA was carried out with Tukey's correction for multiple comparisons (e), or two-way ANOVA was carried out with Sidak's correction for multiple comparisons (l). Data are representative of three independent experiments (b, d). NS, not significant.

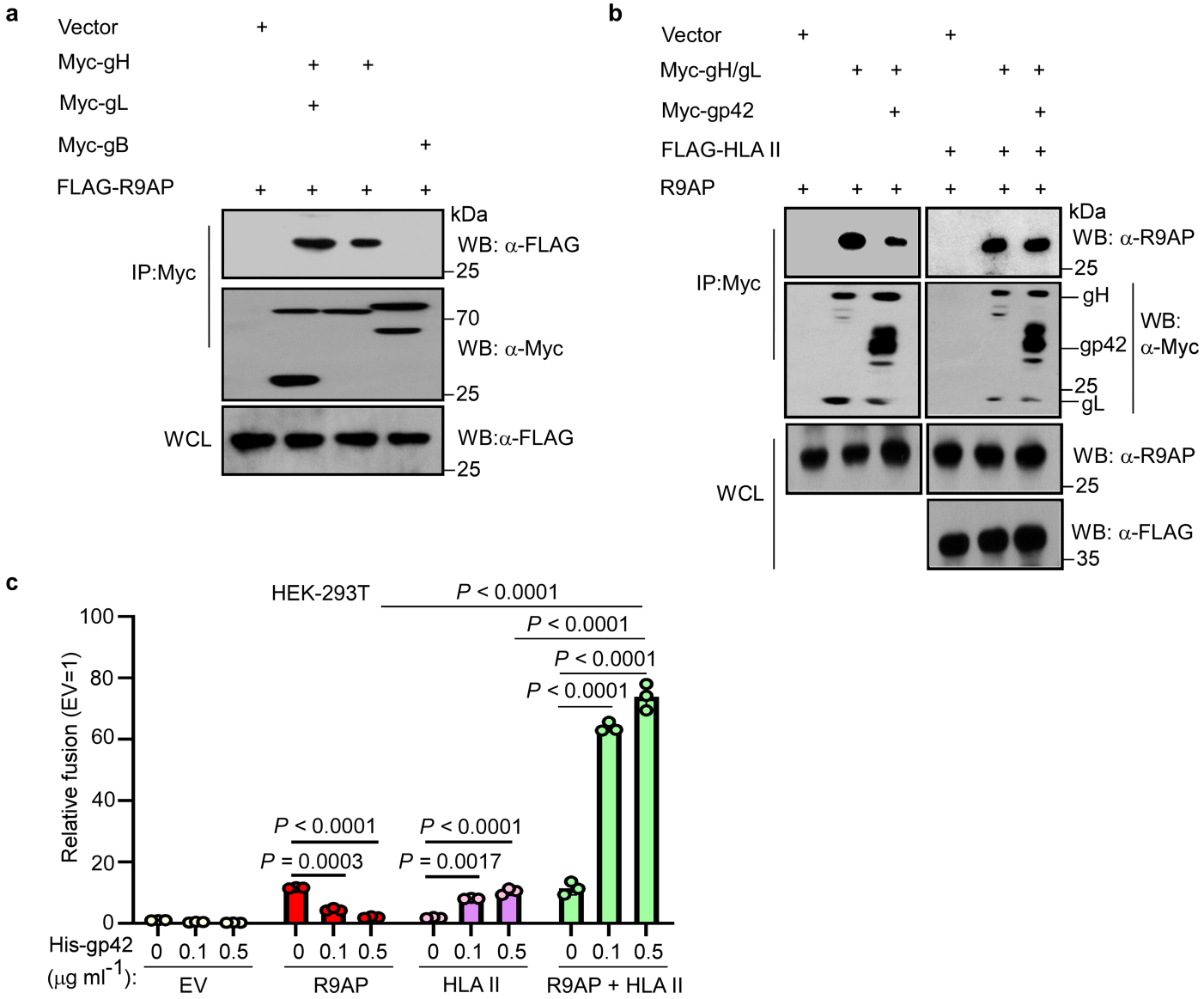

Extended Data Fig. 5 | R9AP interacts with gH and gH/gL and cooperates with gp42-receptor HLA II. a, HEK-293T cells were transfected with FLAG-R9AP, Myc-gH, and Myc-gL, Myc-gH alone, or Myc-gB and then lysed. The cell lysate containing FLAG-R9AP was incubated with the cell lysate containing Myc-gH and Myc-gL, Myc-gH alone, or Myc-gB, then immunoprecipitated with an antibody against Myc followed by WB analysis with the indicated antibody. **b**, HEK-293T cells were co-transfected with R9AP and EV, Myc-gH/gL, Myc-gH/gL/gp42, or Myc-gH/gL/gp42, and FLAG-HLA II (HLA-DR1). Cells were lysed and immunoprecipitated with antibodies against Myc, followed by WB analysis with the indicated antibodies. **c**, Cell-based EBV fusion assay by co-culture of R9AP, HLA II (HLA-DR1), or R9AP/HLA II (HLA-DR1) overexpressed HEK-293T cells, HEK-293T cells transfected with gB/gH/gL, and His-gp42 protein. Data are mean ± S.E.M. (n = 3 biological replicates). Two-way ANOVA was carried out with Sidak's correction for multiple comparisons. ($P < 0.0001$) Data are representative of two independent experiments (a-c).

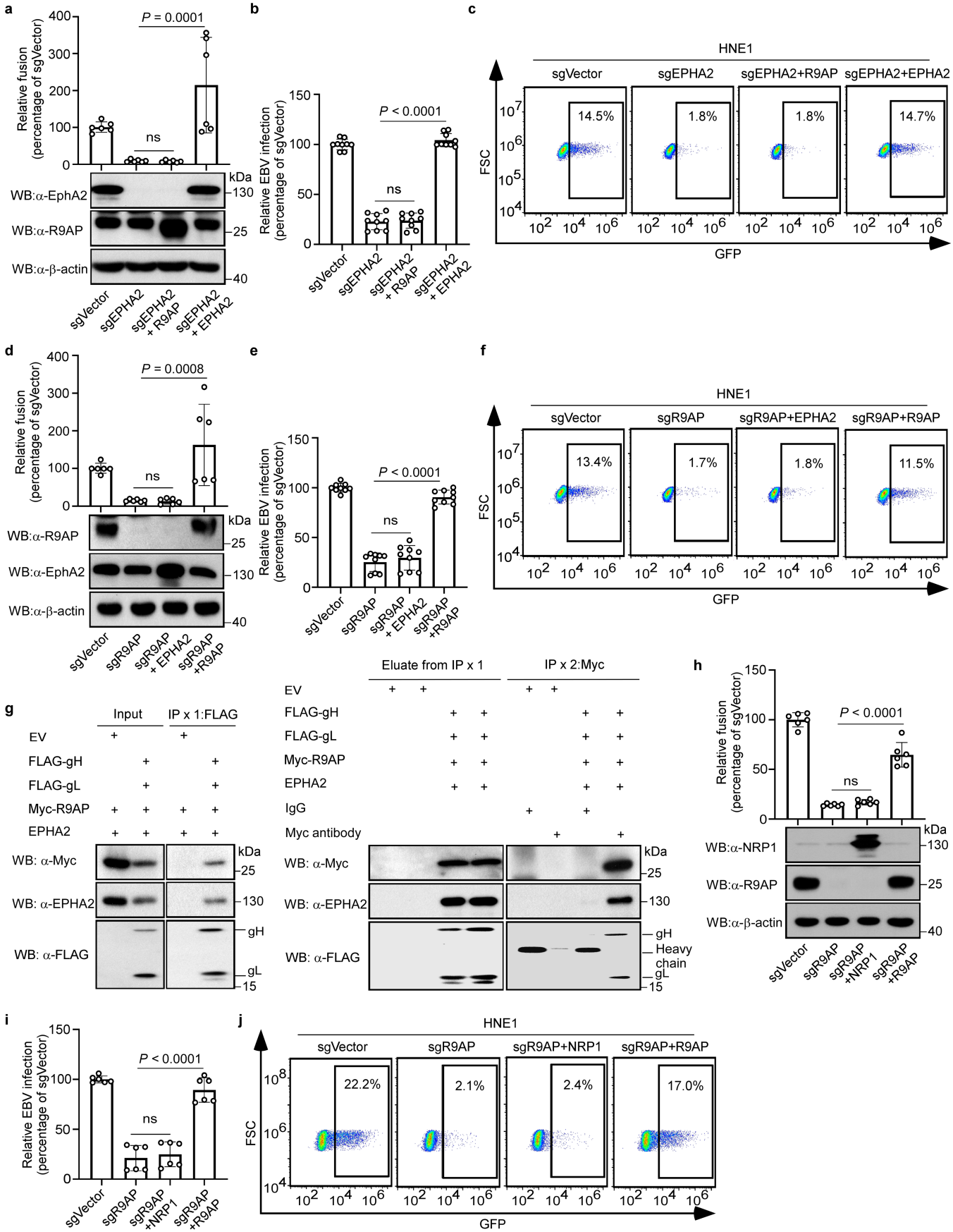

Extended Data Fig. 6 | See next page for caption.

Extended Data Fig. 6 | R9AP, EPHA2, and NRP1 are not redundant for EBV infection of epithelial cells. a-**c**, Cell-based EBV fusion assay by co-culture of sgVector transfected HNE1 cells, EPHA2 knockout HNE1 cells, R9AP overexpressed while EPHA2 knockout HNE1 cells or EPHA2 rescued EPHA2 knockout HNE1 cells, and HEK-293T cells transfected with gH/gL/gB (a). EBV infection efficiency was analyzed by flow cytometry (c) and quantified (b) in the above-indicated HNE1 cells. **d**-**f**, Cell-based EBV fusion assay by co-culture of sgVector transfected HNE1 cells, R9AP knockout HNE1 cells, EPHA2 overexpressed while R9AP knockout HNE1 cells or R9AP rescued R9AP knockout HNE1 cells, and HEK-293T cells transfected with gH/gL/gB (d). EBV infection efficiency was analyzed by flow cytometry (f) and quantified (e) in the above-indicated HNE1 cells. **g**, HEK-293T cells were transfected with Myc-R9AP, EPHA2 together with FLAG-gH/gL or EV, lysed, and immunoprecipitated with antibody against FLAG as indicated IPx1:FLAG. The immunoprecipitated proteins were eluted by FLAG peptide and re-immunoprecipitated with antibody against Myc as indicated IPx2: Myc, followed by WB analysis with indicated antibodies. Data are representative of two independent experiments. **h**-**j**, Cell-based EBV fusion assay by co-culture of sgVector transfected HNE1 cells, R9AP knockout HNE1 cells, NRP1 overexpressed while R9AP knockout HNE1 cells or R9AP rescued R9AP knockout HNE1 cells, and HEK-293T cells transfected with gH/gL/gB (h). EBV infection efficiency was analyzed by flow cytometry (j) and quantified (i) in the above-indicated HNE1 cells. Two independent experiments in triplicates (n = 6) and mean and S.E.M. of those n = 6 were used (a, d, h, i), or three independent experiments in triplicates (n = 9) and mean and S.E.M. of those n = 9 were used (b, e). One-way ANOVA was carried out with Tukey's correction for multiple comparisons. Data are representative of three (c, f) or two (j) independent experiments.

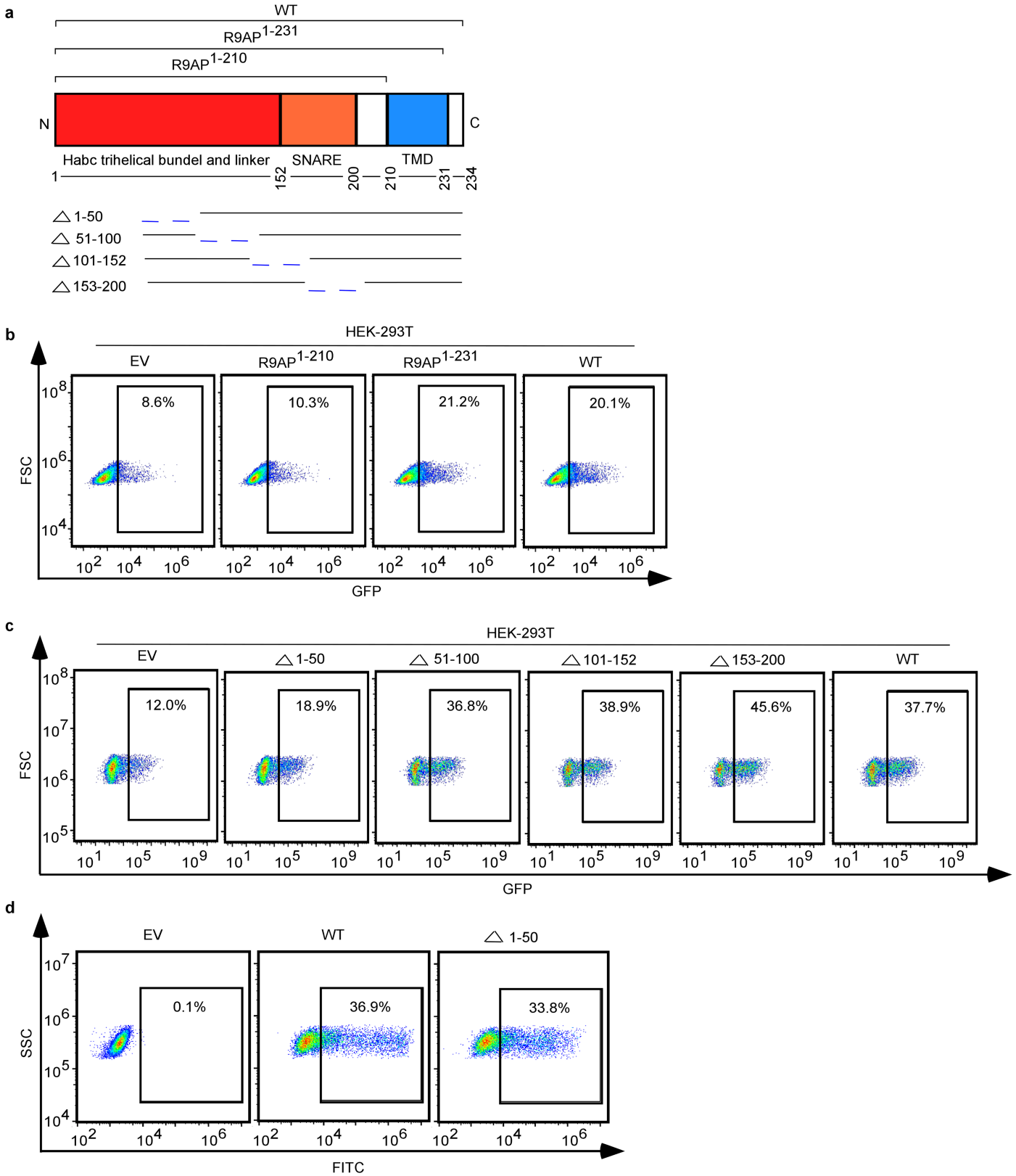

Extended Data Fig. 7 | Functional domains of R9AP. a, Schematic representation of R9AP wild-type (WT), R9AP$^{1\text{-}210}$, R9AP$^{1\text{-}231}$, R9AP mutants deleted of amino acids 1-50 (Δ1-50), 51-100 (Δ51-100), 101-152 (Δ101-152), or 153-200 (Δ153-200). **b, c**, EBV infection efficiency was analyzed in EV, R9AP$^{1\text{-}210}$, R9AP$^{1\text{-}231}$, or WT transiently transfected HEK-293T cells (b), as well as EV, Δ1-50, Δ51-100, Δ101-152, Δ153-200 or WT transiently transfected HEK-293T cells (c). **d**, EV, N-terminus FLAG-tagged WT or Δ1-50 R9AP mutant was transiently transfected into HEK-293T cells. Cells were stained with FITC-FLAG antibody and analyzed by flow cytometry. Data are representative of three independent experiments (b-d).

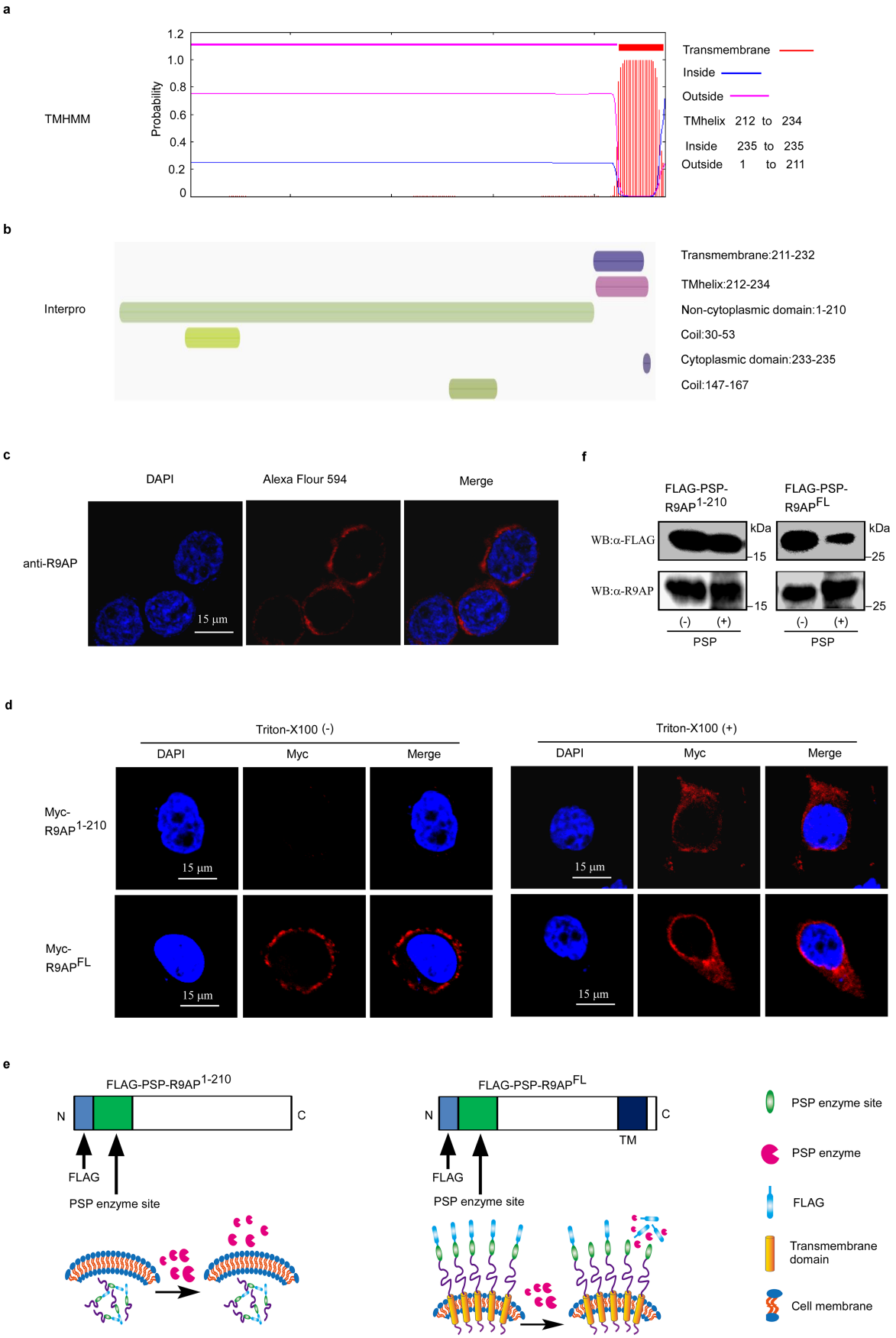

Extended Data Fig. 8 | See next page for caption.

Extended Data Fig. 8 | N-terminus of R9AP locates at cell surface. **a, b**, Prediction of R9AP localization by using TMHMM (a) or InterPro (b). **c**, HK1 cells were fixed and then incubated with antibody targeting N-terminal of R9AP and Alexa Flour 594-labelled goat antibody (red), nuclei were stained with DAPI (blue). **d**, HNE1 cells transfected with Myc-R9AP$^{1\text{-}210}$ or Myc-R9AP^{FL} expression plasmid for 24 h, fixed and treated with or without Triton X-100, followed by incubation with the antibody specific for Myc tag and Alexa Flour 594-labelled goat antibody (red), nuclei were stained with DAPI (blue). **e, f**, PreScission protease (PSP) cleavage site was inserted between the FLAG tag and the N-terminal end of R9AP$^{1\text{-}210}$ (FLAG-psp-R9AP$^{1\text{-}210}$) or R9AP^{FL} (FLAG-psp-R9AP^{FL}) expressing plasmid. Cells transfected with indicated plasmid were cultured for 24 h followed by PSP treatment to remove FLAG located at outside of cells. The schematic was used to show that FLAG tag is removed by the PSP when it is located outside the cell whereas it is retained when located in the cytoplasm (e). WB was used to detect the R9AP or FLAG tag after adding PSP enzyme (f). Data are representative of three (c) two (d, f) independent experiments.

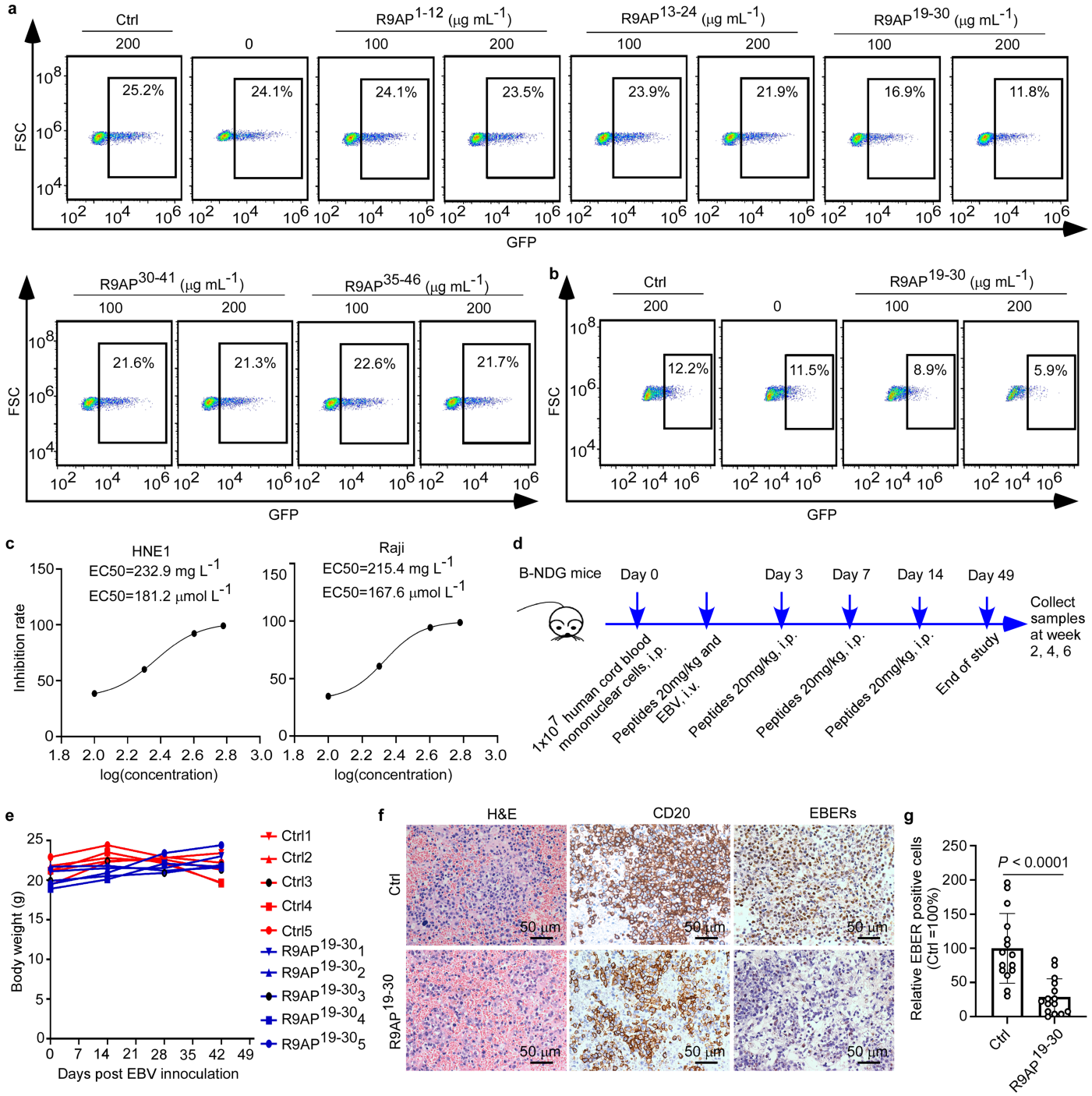

Extended Data Fig. 9 | R9AP peptide inhibits EBV infection in vitro and in vivo. a, b, EBV was pretreated with R9AP$^{1-12}$, R9AP$^{13-24}$, R9AP$^{19-30}$, R9AP$^{30-41}$, R9AP$^{35-46}$, or Ctrl peptide, then added to HNE1 cells (a), R9AP$^{19-30}$ or Ctrl pretreated EBV was added to Raji cells (b). EBV infection efficiency was analyzed by flow cytometry. **c**, EBV was pretreated with R9AP$^{19-30}$ at a concentration of 0, 50, 100, 200, or 400 μg mL^{-1}, then added to HNE1 or Raji cells. EBV infection efficiency was analyzed by flow cytometry, and the EC50 of R9AP$^{19-30}$ was determined. **d**, Schematic representation of in vivo EBV infection using humanized B-NDG mice. **e**, The body weight of humanized B-NDG mice treated with R9AP$^{19-30}$ or Ctrl peptide at indicated time points (Ctrl, n = 5 mice; R9AP$^{19-30}$, n = 5 mice). **f**, Representative images of spleen tissue sections of humanized B-NDG mice infected with EBV and treated with R9AP$^{19-30}$ or Ctrl peptide stained with hematoxylin-eosin staining (H& E), anti-human CD20, or hybridized with EBV EBERs probe. Scale bar=50 μm. The samples' representative images were detected (Ctrl, n = 5 mice; R9AP$^{19-30}$, n = 5 mice). **g**, The proportion of EBERs-positive cells in the spleen of EBV-infected and R9AP$^{19-30}$ or Ctrl peptide-treated humanized B-NDG mice were independently evaluated by three pathologists. Three independent evaluation of each mouse (n = 15) and mean and S.E.M. of those n = 15 were used, two-tailed unpaired Student's *t*-test (Ctrl, n = 5 mice; R9AP$^{19-30}$, n = 5 mice). ($P < 0.0001$) Data are representative of three (a, b) two (c) independent experiments.

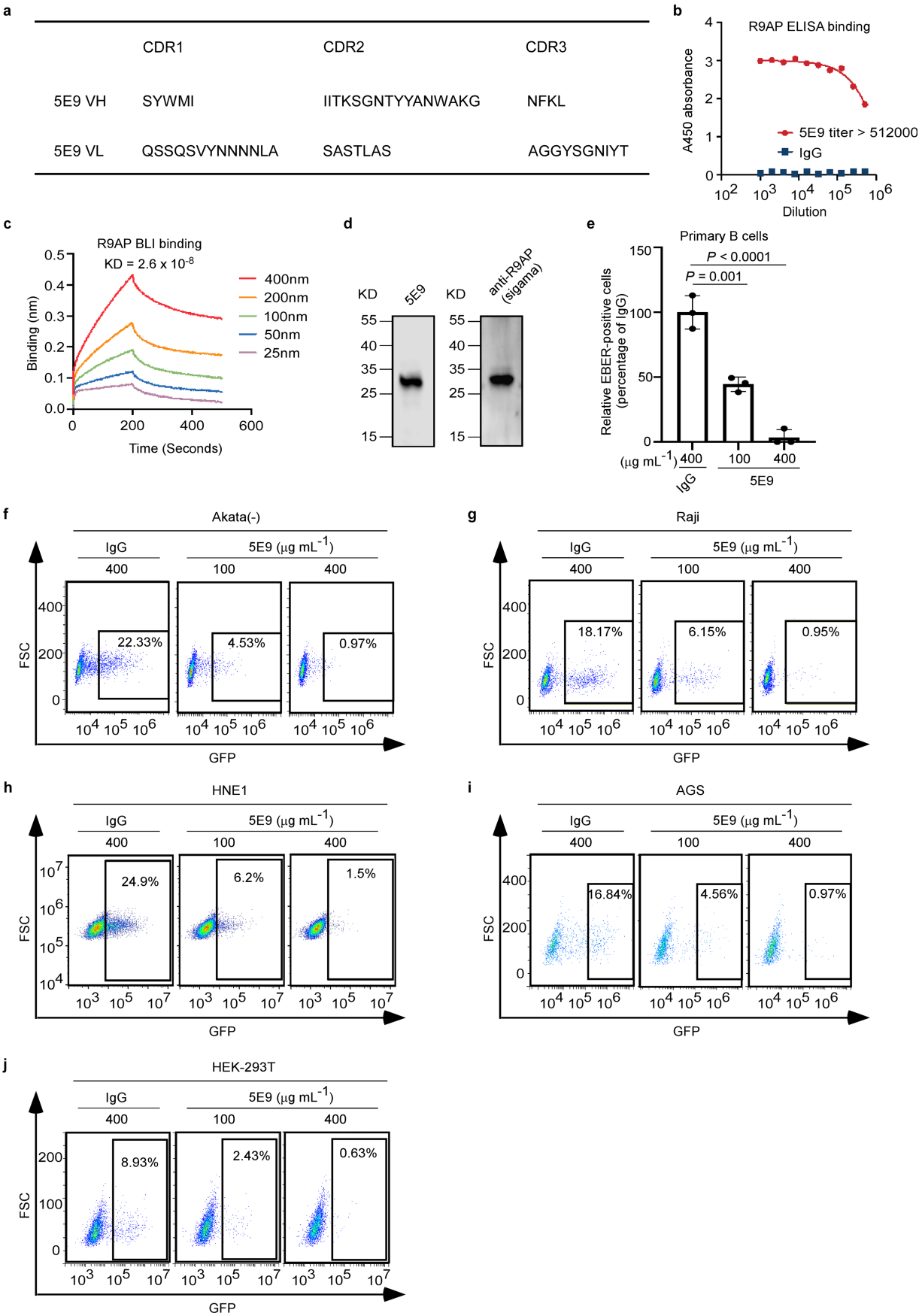

Extended Data Fig. 10 | See next page for caption.

Extended Data Fig. 10 | Characterization of the anti-R9AP monoclonal antibody 5E9 and its effects on blocking EBV infection. a, Complementarity determining regions (CDR) details for the anti-R9AP monoclonal antibody 5E9 antibody. **b**, ELISA binding for 5E9 and control antibody to $R9AP^{1-210}$. The A450 signals were from triplicate wells and the mean signal were presented. **c**, BLI binding assay for 5E9 to $R9AP^{1-210}$. 5E9 were captured onto ProA biosensors and assayed for binding to $R9AP^{1-210}$. **d**, WB for 5E9 binding to R9AP in comparison to commercial antibody. HEK-293T cells were transfected with FLAG-R9AP. Cells were lysed and immunoprecipitated with 5E9 or anti-R9AP antibody (Cat #HPA049791, Sigma). **e**, Primary B cells were pretreated with anti-R9AP monoclonal antibody (5E9), then infected with EBV. The proportion of EBERs-positive cells were independently evaluated by three pathologists. Each pathologist counted 3 representative high-power fields (×40 objective) per sample, with approximately 100 cells/field, and obtained a mean value. Bars represent proportion of EBERs-positive cells. Data are mean ± S.E.M. and representative of two independent experiments (n = 3). **f-j**, Akata, Raji, HNE1, AGS and HEK-293T cells were pretreated with anti-R9AP monoclonal antibody (5E9), then infected with EBV. EBV infection efficiency was analyzed by flow cytometry. Data are representative of two (b-d) or three independent experiments (f-j).

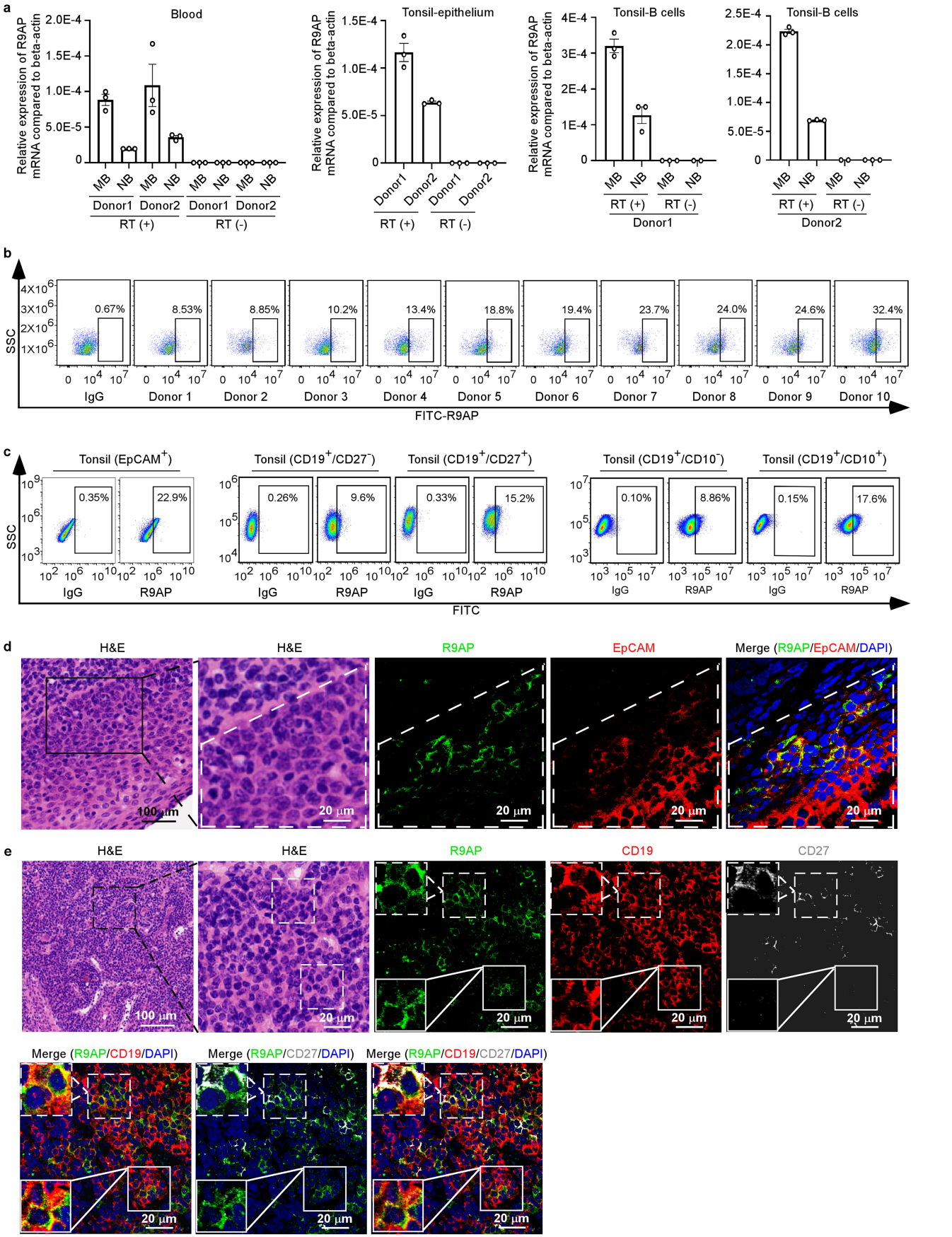

Extended Data Fig. 11 | See next page for caption.

Extended Data Fig. 11 | R9AP expression in human tonsil and blood tissues. **a**, RT-qPCR was used to quantify the mRNA level of the R9AP in tonsil epithelial cells of 2 donors and memory B cells and naïve B cells from 2 donor's blood and tonsil tissues. Data are mean ± S.E.M. (n = 3 biological replicates) and are from 2 donors. **b**, Blood PBMC were co-stained with CD19/R9AP antibody and analyzed by flow cytometry. Results are representative of 10 donors. **c**, Cells from tonsil tissues were co-stained with EpCAM/R9AP, CD19/CD27/R9AP, or CD19/CD10/R9AP antibody and analyzed by flow cytometry. Results are representative of 3 donors. **d, e**, Epithelium, and lymphoid tissues from tonsil were stained with hematoxylin-eosin staining (H&E), co-stained with R9AP (imaged as green) antibody and EpCAM (imaged as red) antibody, or co-stained with R9AP (imaged as green), CD19 (imaged as red) and CD27 (imaged as gray) antibodies, nuclei were stained with DAPI (blue), and analyzed by immunofluorescence. Epithelial cells were delineated by the dotted line (d). The white dotted areas indicated $CD19^+CD27^+R9AP^+$ cells and were magnified 3 times, and the white solid areas indicated $CD19^+CD27^-R9AP^+$ cells (e). Results are representative of 2 donors.

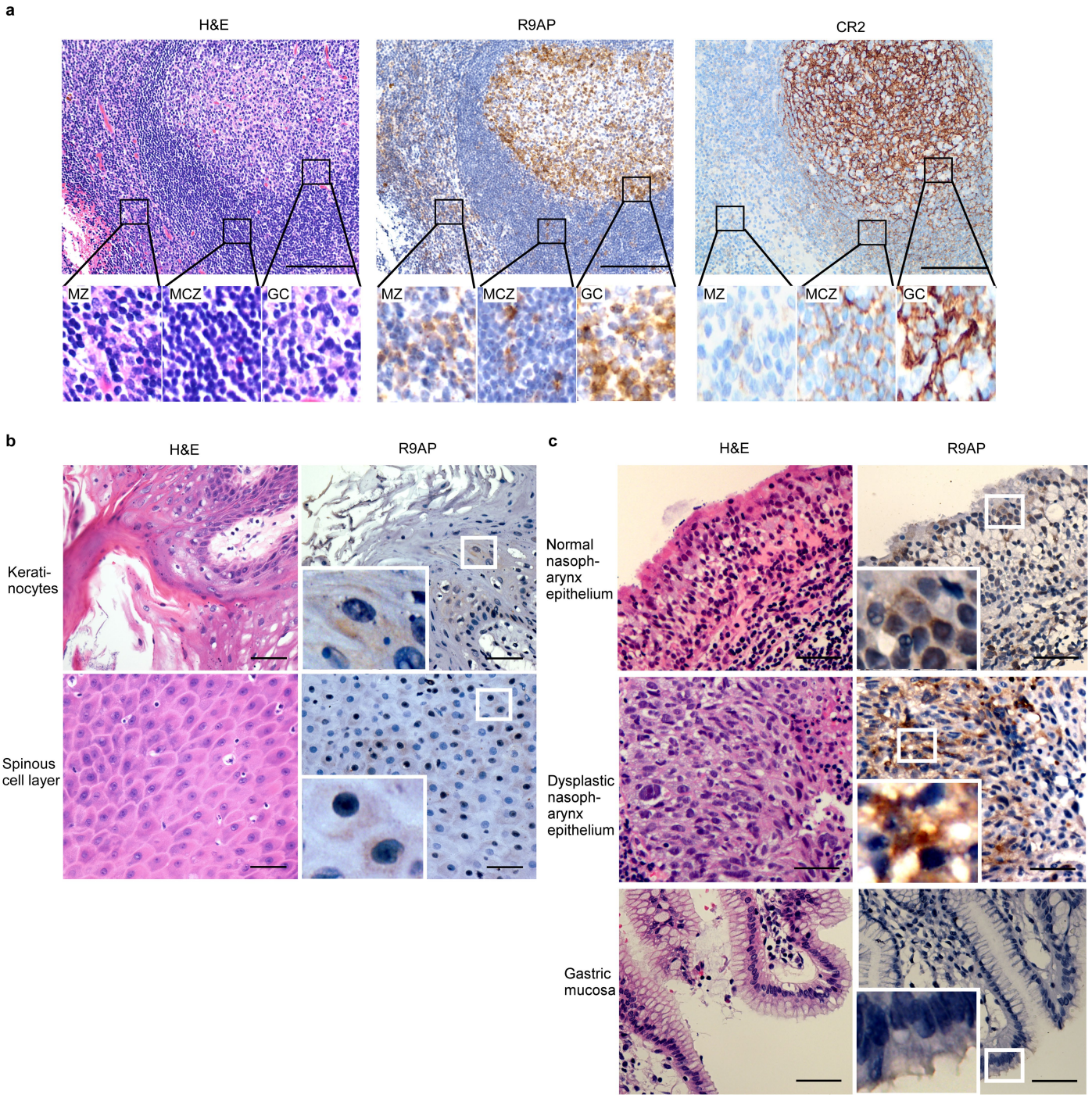

Extended Data Fig. 12 | R9AP expression in human lymphoid, tongue, floor of mouth, nasopharynx epithelium and gastric mucosa tissues. a, Human lymphoid tissues (n = 3) were stained with hematoxylin-eosin (H&E) (left), R9AP antibody (middle), and CR2 antibody (right). Images of insets were magnified 4 times. GC: germinal center; MCZ: mantle cell zone; MZ: marginal zone. Scale bars: 100 μm. **b**, The keratinocytes and spinous cell layer of human tongue (n = 5) and floor of the mouth tissues (n = 5) were stained with hematoxylin-eosin (H&E) (left) and R9AP antibody (right). Images of insets were magnified 4 times. Scale bars: 50 μm. **c**, Tissues of human normal (n = 5) and dysplastic nasopharynx epithelium (n = 4) and normal gastric mucosa (n = 5) were stained with H& E (top row) and R9AP antibody (bottom row). Images of insets were magnified 4 times. Scale bar=50 μm. Representative images from the samples detected (a-c).

nature portfolio

Corresponding author(s): Mu-Sheng Zeng

Last updated by author(s): 2025-3-5

Reporting Summary

Nature Portfolio wishes to improve the reproducibility of the work that we publish. This form provides structure for consistency and transparency in reporting. For further information on Nature Portfolio policies, see our Editorial Policies and the Editorial Policy Checklist.

Statistics

For all statistical analyses, confirm that the following items are present in the figure legend, table legend, main text, or Methods section.

n/a	Confirmed
☐	☒ The exact sample size (*n*) for each experimental group/condition, given as a discrete number and unit of measurement
☐	☒ A statement on whether measurements were taken from distinct samples or whether the same sample was measured repeatedly
☐	☒ The statistical test(s) used AND whether they are one- or two-sided *Only common tests should be described solely by name; describe more complex techniques in the Methods section.*
☒	☐ A description of all covariates tested
☐	☒ A description of any assumptions or corrections, such as tests of normality and adjustment for multiple comparisons
☐	☒ A full description of the statistical parameters including central tendency (e.g. means) or other basic estimates (e.g. regression coefficient) AND variation (e.g. standard deviation) or associated estimates of uncertainty (e.g. confidence intervals)
☐	☒ For null hypothesis testing, the test statistic (e.g. *F*, *t*, *r*) with confidence intervals, effect sizes, degrees of freedom and *P* value noted *Give P values as exact values whenever suitable.*
☒	☐ For Bayesian analysis, information on the choice of priors and Markov chain Monte Carlo settings
☒	☐ For hierarchical and complex designs, identification of the appropriate level for tests and full reporting of outcomes
☒	☐ Estimates of effect sizes (e.g. Cohen's *d*, Pearson's *r*), indicating how they were calculated

Our web collection on statistics for biologists contains articles on many of the points above.

Software and code

Policy information about availability of computer code

Data collection	1. qPCR: Bio-Rad CFX Maestro 1.1; 2. FCM: Beakman Gallios, CytExpert (Version 2.4.0); 3. WB: Image Lab (Version 5.2.1), CanonScan LiDE110; 4. Microscopic image: OLYMPUS FV1000; 5. BLI: Octet Red 96 instrument (18-1127; ForteBio);
Data analysis	1. Graphing and statistical analysis: Graphpad Prism 8.3; 2. Cytometry data analysis: FlowJo vlO.5.3; 3. Microarray data processing: Genespring (version 9); 4. Microarray heatmap: Graph pad Prism 8.3; 5. BLI: ForteBio data analysis software (Version 8.0); 6. Prediction of R9AP localization:TMHMM software (Version 2.0) and InterPro 7. Figures were assembled using Adobe Illustrator (25.2.3).

For manuscripts utilizing custom algorithms or software that are central to the research but not yet described in published literature, software must be made available to editors and reviewers. We strongly encourage code deposition in a community repository (e.g. GitHub). See the Nature Portfolio guidelines for submitting code & software for further information.

Data

Policy information about availability of data

All manuscripts must include a data availability statement. This statement should provide the following information, where applicable:

- Accession codes, unique identifiers, or web links for publicly available datasets
- A description of any restrictions on data availability
- For clinical datasets or third party data, please ensure that the statement adheres to our policy

There are no restrictions on data availability in this manuscript. All data is available in the main text or extended data. The uncropped WB image were shown in Supplementary information. Raw data for animal-related experiments in main and extended Figures are provided as source data. Microarray data presented in this study is available on NCBI GEO repository (GSE159958). The key raw data of all the functional experiments of the main figures in this work has been deposited onto the Research Data Deposit public platform (www.researchdata.org.cn) with the approval number RDDB2020001025. All other data are available from the corresponding author on reasonable request.

Research involving human participants, their data, or biological material

Policy information about studies with human participants or human data. See also policy information about sex, gender (identity/presentation), and sexual orientation and race, ethnicity and racism.

Reporting on sex and gender	Sex and gender is not considered in the study design, participant inclusion and grouping.
Reporting on race, ethnicity, or other socially relevant groupings	Not applicable.
Population characteristics	Cohort 1: Histological specimens from patients with benign diseases of tongue (eight samples), floor of mouth (five samples), lymphoid (eight samples) and chronic tonsillitis (ten samples), and with malignant diseases of nasopharyngeal carcinoma(eleven samples), EBV-positive gastric carcinoma (nine samples), EBV-positive B cell lymphoma (seven samples), liver tissues(three samples), lung tissues (three samples), thyroid tissues (three samples), normal nasopharynx epithelium tissues (five samples), dysplastic nasopharynx epithelium tissues (four samples), normal gastric mucosa tissues (five samples) were obtained from Sun Yat-sen university cancer center. The patient age range: 20-70 years, with a male-to-female ratio of 1.1:1. Cohort 2: Human cord blood (five samples) was obtained from Guangzhou Women and Children's Medical Center (China). The patient age range: 24-36 years, all were female. Cohort 3: Periphery blood samples (21 samples) were obtained from Sun Yat-sen university cancer center. The patient age range: 20-50 years, with a male-to-female ratio of 1:1.2.
Recruitment	No recruitment strategy was employed in this study. All patients were diagnosed with indicated benign diseases or malignantdiseases by the pathologist. Informed written consent was obtained prior to surgery. We don't anticipate any self-selectionbias.
Ethics oversight	Written informed consents forms were signed by all the donors and patients. All the utilization of human samples was approved by the institutional review board of each institution taking part in the project. Human cord blood was obtained from Guangzhou Women and Children's Medical Center (China) , approved by the Committee on the Ethics of Guangzhou Women and Children's Medical Center. Human tissues including lymphoid tissues, floor of mouth, tongue, lymph node, liver, lung, thyroid, blood, tonsil, nasopharynx epithelium, gastric mucosa, and tumor tissues were collected from Sun Yat-sen University Cancer Center, approved by the Committee on the Ethics of Sun Yat-sen University Cancer Center.

Note that full information on the approval of the study protocol must also be provided in the manuscript.

Field-specific reporting

Please select the one below that is the best fit for your research. If you are not sure, read the appropriate sections before making your selection.

☒ Life sciences ☐ Behavioural & social sciences ☐ Ecological, evolutionary & environmental sciences

For a reference copy of the document with all sections, see nature.com/documents/nr-reporting-summary-flat.pdf

Life sciences study design

All studies must disclose on these points even when the disclosure is negative.

Sample size	No statistical tests were used to determine sample size. Sample size in this study is determined based on previous studies in Nature as reference and all sample sizes for experiments in this study are sufficient to perform statistical presentation and examination according to the used statistical method mandatory requirement and previous study outcomes. Sample sizes are indicated in figure legend;For in vitro experiments, sample sizes were determined based on the numbers required to achieve statistical significance using indicated statistics, but with a minimum of two independent experiments except Extended Data Fig. la, lb, to ensure data reproducibility; For in vivo experiments, we used five immunodeficient B-NDG mice per group and followed the 3R's of animal research; For IHC assay of R9AP expression in human

tissues, five cases of human tongue, five cases of floor of mouth, five cases of lymphoid, five cases of nasopharyngeal carcinoma, three cases of gastric carcinoma, four cases of EBV-positive B cell lymphoma, three cases of tonsil, five cases of normal nasopharynx epithelium, four cases of dysplastic nasopharynx epithelium, five cases of normal gastric mucosa tissues were included;For WB assay of R9AP expression in human tissues, three cases of tongue, three cases of lymph node, three cases of gastric mucosa, three cases of liver, three cases of lung, three cases of thyroid, six cases of EBV-positive lymphoma, six cases of nasopharyngeal carcinoma, three cases of EBV-positive gastric carcinoma were included;For sgRNA, R9AP peptides and R9AP monoclonal antibody blocking assays in primary B cells, PBMCs from nine healthy donors were collected;For detection of R9AP expression by qRT-PCR, two cases of PBMCs from healthy donors and two cases of tonsil tissues from tonsillitis patients were collected; for detection of R9AP expression by IF assays, two cases of tonsil tissues from tonsillitis patients were collected; for detection of R9AP expression by flow cytometry, ten cases of PBMCs from healthy donors and three cases of tonsil tissues from tonsillitis patients were collected.

Data exclusions

No data were excluded.

Replication

All in vitro experiments were performed with at least two biological or technical replicates shown in figure legends, and all in vitro experiments were repeated and the repeated times for each experiment was stated in figure legends; For in vivo experiments, we used five immunodeficient B-NDG mice per group and the statistical significance was shown in figure legends; For human tissue experiments, we used at least two samples to yield the results, and the sample number was shown in indicated figure legends; All attempts to replicate results were successful.

Randomization

Randomization was applied wherever possible. All the in vitro experiments were randomly assigned to experimental conditions. For example, during flow cytometry analyses, samples were processed and subjected to the CytExpert in random orders. All microscopic images were randomly taken throughout the slide of each sample. Mice were sex- and age-matched and grouped randomly according to the genotype. Otherwise, randomization was not performed. For example, when performing immunoblotting, samples needed to be loaded in a specific order to generate the final figures.

Blinding

During the histological analyses, the sample collection and processing were labelled as code names. The fields of view were chosen on a random basis and independently evaluated by three pathologists who did not participate in sample collection and processing. In other experiments, Blinding was not necessary, as most datawas acquired by unbiased automated means.

Reporting for specific materials, systems and methods

We require information from authors about some types of materials, experimental systems and methods used in many studies. Here, indicate whether each material, system or method listed is relevant to your study. If you are not sure if a list item applies to your research, read the appropriate section before selecting a response.

Materials & experimental systems

n/a	Involved in the study
☐	☒ Antibodies
☐	☒ Eukaryotic cell lines
☒	☐ Palaeontology and archaeology
☐	☒ Animals and other organisms
☒	☐ Clinical data
☒	☐ Dual use research of concern
☒	☐ Plants

Methods

n/a	Involved in the study
☒	☐ ChIP-seq
☐	☒ Flow cytometry
☒	☐ MRI-based neuroimaging

Antibodies

Antibodies used

IP: ANTI-FLAG M2 Gel (A2220, Sigma-Aldrich, 1:200), Anti-c-Myc Agarose Affinity Gel (A7470, Sigma-Aldrich, 1:200), CL59 antibody (generated based on the reported sequence by ourselves, 1:200 and 1:100), AMMO1 (generated based on the reported sequence by ourselves, 1:200 and 1:100).
WB: Anti-R9AP (HPA049791; Sigma-Aldrich, 1:1000), Anti-Myc tag (M5546; Sigma-Aldrich, 1:1000), Anti-FLAG (F3165; Sigma-Aldrich, 1:1000), Anti-CNGA1 (DF3929, Affinity, 1:1000), Anti-GPR1 (DF2720, Affinity, 1:1000), Anti-SLC26A9 (SAB2105558, Sigma-Aldrich, 1:1000), Anti-beta-actin (8H10D10, 3700, CellS ignaling, 1:1000), Anti-His tag (D3I1O, 12698, Cell Signaling, 1:1000), Anti-EphA2 (D4A2, 6997, Cell Signaling, 1:1000), Anti-NRP1 (446921, AF3870, R&D Systems, 1:1000).
IF or FCM: Anti-R9AP (CSB-PA765076LA01HU, CUSABIO, IF 1:100, FCM 1:200), CD27-AF700 (302814, BioLegend, IF 1:100, FCM 1:200), mouse CD27-PE (LG.3A10 clone,BioLegend, IF 1:100, FCM 1:200), EpCAM-AF594 (118222, BioLegend, IF 1:100, FCM 1:200), CD19-AF647 (302220, BioLegend, IF 1:100, FCM 1:200), CD10-PE (312204, BioLegend, 1:200), anti-human IgG antibody (CSB-PA00120E1Rb; CUSABIO, 1:200).
IHC: Anti-R9AP (HPA049791; Sigma-Aldrich), CR2 (EP64, ZSGB-BIO, 1:200).
Antibody blocking assay: Anti-R9AP (5E9, generated by ourselves, 1:80 and 1:20).
EBV label: 72A1 (generated based on the reported sequence by ourselves, 1:200).

Validation

The commercially available antibodies were validated by the company. The sequences of the antibodies generated by ourselves were validated by PCR, as well as antibodies validated by BLI with certain antigen.

Eukaryotic cell lines

Policy information about cell lines and Sex and Gender in Research

Cell line source(s)	HEK-293T, Raji, BJAB and Daudi were purchased form ATCC; We thank Dr. Maria Masucci (Karolinska Institute, Sweden) for providing the Akata cell line; Dr. Quen-Tin Liu (Sun Yat-sen University, Guangzhou, China) for providing the CNE1 cell line; Dr. Sai-Wah Tsao (University of Hong Kong, Hong Kong SAR) for providing the HNE1 and HK1 cell lines; Dr. Qian Tao (Chinese University of Hong Kong, Hong Kong SAR) for providing the AGS cell line; Dr. Xu Rui-Hua (Sun Yat-sen University, Guangzhou, China) for providing the MKN74 cell line.
Authentication	Cell lines HEK-293T, AGS, MKN74, HK1, Raji, Akata, BJAB, Daudi, NPECl-Bmil and NPEC2-Bmil were authentication by STRanalysis before use in this study. There are only few nasopharyngeal carcinoma cell lines available and we chose HNE1 and CNE1 for the functional experiments besides the authenticated HK1 cells. HNE1 and CNE1 is not listed in ICLAC database, but may be contaminated by Hela cells. However, unlike Hela cells , which are resistant to EBV infection, CNE1 cells are susceptible to EBV infection in vitro. Therefore, we used HK1, HNE1 and CNE1, and all these cells showed similar results in this study, which demonstrated that R9AP is acommon receptor for EBV infection in both epithelial cells and B cells.
Mycoplasma contamination	Mycoplasma tests were performed monthly and confirmed to be negative by PCR and gel electrophoresis.
Commonly misidentified lines (See ICLAC register)	Not applicable.

Animals and other research organisms

Policy information about studies involving animals; ARRIVE guidelines recommended for reporting animal research, and Sex and Gender in Research

Laboratory animals	Ten 4 to 5-week-old female immunodeficient NOD/SCID gamma (NDG) mice were purchased from BIOCYTOGEN (China); 2 3-month-old New Zealand white rabbits were purchased from Genescript (China). Mice were housed with free acess to water and standard diet under pathogen-free conditions. The light was on from 8:00 to 20:00, with temperature kept at 21-24 Celsius degree and humidity at 40-70%.
Wild animals	The study did not involve wild animals.
Reporting on sex	Sex is not predetermined in this study, not relevant to any conclusion and not involved in experimental design.
Field-collected samples	The study did not involve samples collected form field.
Ethics oversight	All animal experiments with infectious EBV were performed in the animal biosafety level 2 facilities at Sun Yat-sen UniversityZhongshan School of Medicine, which was approved by the Committee on the Ethics of Animal Experiments of Sun Yat-senUniversity. The animal studies were carried out in strict accordance with the recommendations promulgated in the Guide for theCare and Use of Laboratory Animals of the Ministry of Science and Technology of the People's Republic of China.

Note that full information on the approval of the study protocol must also be provided in the manuscript.

Plants

Seed stocks	Not applicable.
Novel plant genotypes	Not applicable.
Authentication	Not applicable.

Flow Cytometry

Plots

Confirm that:

☒ The axis labels state the marker and fluorochrome used (e.g. CD4-FITC).

☒ The axis scales are clearly visible. Include numbers along axes only for bottom left plot of group (a 'group' is an analysis of identical markers).

☒ All plots are contour plots with outliers or pseudocolor plots.

☒ A numerical value for number of cells or percentage (with statistics) is provided.

Methodology

Sample preparation	Cell lines were routinely cultured prior to EBV infection, samples were filtered prior to staining, and kept on ice duringstaining, all fluorescent antibodies were aliquotted. Staining samples were protected from light throughout; For detectoin ofR9AP expression in human tonsil tissues, we collect the tissues and digest with DNAse 1 plus Collagenase IV.
Instrument	Beckman Gallios, Beckman CytoFLEX S
Software	FlowJo vlO.5.3, Graphpad Prism 8.3
Cell population abundance	No sorting were performed.
Gating strategy	The non-infected cells or anti-human IgG antibody treated cells were analyzed, and set as negative cell population.

☒ Tick this box to confirm that a figure exemplifying the gating strategy is provided in the Supplementary Information.